Characterization of the single *FERONIA* homolog in *Marchantia polymorpha* reveals an ancestral role of *Cr*RLK1L receptor kinases in regulating cell expansion and morphological integrity

Martin A. Mecchia[1#], Moritz Rövekamp[1#+], Alejandro Giraldo-Fonseca[1], Dario Meier[1], Philippe Gadient[1], John L. Bowman[2], and Ueli Grossniklaus[1*]

[1]Department of Plant and Microbial Biology and Zurich-Basel Plant Science Center, University of Zurich, 8008 Zurich, Switzerland

[2]School of Biological Sciences, Monash University, Clayton, Melbourne, Victoria 3800, Australia

[+] Current Affiliation: Department of Aquatic Ecology, EAWAG, 8600 Duebendorf, Switzerland

# These authors contributed equally to the manuscript.

*Author for correspondence: grossnik@botinst.uzh.ch

Short tittle: Deciphering the ancestral role of *Cr*RLK1L receptors in land plants

Summary

Plant cells are surrounded by a cell wall, a rigid structure rich in polysaccharides and glycoproteins. The cell wall is not only important for cell and organ shape, but crucial for intercellular communication, plant-microbe interactions, and as a barrier to the environment. In the flowering plant *Arabidopsis thaliana*, the 17 members of the *Catharanthus roseus* RLK1-like (*Cr*RLK1L) receptor kinase subfamily are involved in a multitude of physiological and developmental processes involving the cell wall, including reproduction, hormone signaling, cell expansion, innate immunity, and various stress responses. Due to genetic redundancy and the fact that individual *Cr*RLK1Ls can have distinct and sometimes opposing functions, it is difficult to assess the primary or ancestral function of *Cr*RLK1Ls. To reduce genetic complexity, we characterized the single *Cr*RLK1L gene of *Marchantia polymorpha*, Mp*FERONIA* (Mp*FER*). Plants with reduced Mp*FER* levels show defects in vegetative development, i.e., rhizoid formation and cell expansion, but also affect male fertility. In contrast, Mp*fer* null mutants and overexpression lines severely affect cell integrity and morphogenesis of the gametophyte. Thus, the *Cr*RLK1L gene family originated from a single gene with an ancestral function in cell expansion and the maintenance of cellular integrity. During land plant evolution, this ancestral gene diversified and was recruited to fulfil a multitude of specialized physiological and developmental and roles in the formation of both gametophytic and sporophytic structures essential to the life cycle of flowering plants.

Key Words

cell wall integrity, cell elongation, *Cr*RLK1L receptor kinases, *Marchantia polymorpha*, signaling pathway evolution

Introduction

The functioning of plant cells is contingent upon the cell wall acting as a barrier between the cell and its environment. This complex matrix of polysaccharides, glycoproteins, and other organic compounds defines the growth and shape of a cell and provides protection against biotic and abiotic stresses [1,2]. Moreover, its stiffness has to resist turgor pressure while also allowing cell expansion during growth. Thus, sensing and controlling cell wall integrity (CWI) is crucial for plant cells and receptor kinases (RKs) play an important role in sensing extracellular cues that activate intracellular pathways. Different RK subfamilies are defined by their extracellular domain (ECD), which is more variable than their transmembrane and kinase domains [3]. Over the last decade, the *Cr*RLK1L subfamily emerged as important CWI sensors [4,5].

Functions have been assigned to 15 of the 17 *Cr*RLK1L members encoded in the *A. thaliana* genome: they are required for cell elongation and cell shape, sensing environmental cues, and cell-cell communication in diverse contexts [6–22]. For instance, *FERONIA* (At*FER*), *THESEUS1* (At*THE1*), *HERCULES1* (At*HERK1*), and At*HERK2* are required for cell elongation as At*fer* single, At*the1*At*herk1* double, and At*the1*At*herk1*At*herk2* triple mutants exhibit stunted growth [7,9–11]. Root hairs burst in mutants affecting At*FER* and *$[Ca^{2+}]_{cyt}$-ASSOCIATED PROTEIN KINASE1* (At*CAP1*)/*ERULUS* (At*ERU*) [12,16]. Moreover, At*FER* plays a role in powdery mildew resistance [11], innate immunity [15,22], calcium signaling [23], phytohormone signaling [10,24–26], and mechano- and heavy metal sensing [20,27]. In most contexts, the *Cr*RLK1Ls tend to promote cellular growth and cell elongation. In contrast, At*THE1* actively inhibits cell elongation in hypocotyls when cell wall perturbations occur, *e.g.*, due to mutations in the cell wall biosynthesis machinery or upon treatment with isoxaben, a cellulose synthesis inhibitor [7,28].

In addition to regulating cellular growth during the vegetative phase of the life cycle, several *Cr*RLK1Ls play a role during fertilization by controlling the growth and reception of the pollen tube. In the female gametophyte, At*FER* is highly expressed in the two synergid cells that flank the egg cell and are important for double fertilization [6,29]. At*FER* is crucial for pollen tube reception and the release of the two sperm cells [6,10,23,30,31], a process also involving two other, redundantly acting synergid-expressed *Cr*RLK1Ls, *AtHERK1* and *ANJEA* (*AtANJ*) [17]. In contrast to these synergid-expressed *Cr*RLK1Ls, four pollen-expressed *Cr*RLK1Ls, named *ANXUR1* (At*ANX1*), At*ANX2, BUDDHA'S PAPER SEAL1* (At*BUPS1*) and At*BUPS2* [8,14,18,32], are redundantly required for pollen tube integrity and tip growth.

To transduce extracellular cues, *Cr*RLK1Ls bind secreted peptides of the RAPID ALKALINIZATION FACTOR (RALF) family [22,32–35], which induce complex formation with members of LORELEI (LRE) family of GPI-anchored proteins [32,35–37]. Hence, it was suggested that at least some *Cr*RLK1Ls act as CWI sensors that coordinate cell elongation in response to changes in the cell wall [38–43].

The 17 *A. thaliana Cr*RLK1Ls act partially redundantly and can have opposite effects on cellular growth (reviewed in [19,41,43,44]). To investigate the original function of *Cr*RLK1Ls, we characterized them in a system with reduced genetic complexity: the liverwort *Marchantia polymorpha* encodes a single *Cr*RLK1L [45,46]. Liverworts represent an early diverging land plant lineage and have been hypothesized to retain, at least in part, characteristics of the earliest land plants [45,47–52]. The presence of similar types of gene families in all plant lineages suggests that the differences in development evolved by co-opting and modifying existing developmental programs and genetic networks, rather than through the evolution of novel genes [47,48,53]. *M. polymorpha* is thus an

ideal system to study the ancestral role of genes and how it was modulated and diversified during land plant evolution [45,54,55].

We refer to the a single *Cr*RLK1L family member encoded in the *M. polymorpha* genome, Mp4g15890 (Mapoly0869s0001), as Mp*FERONIA* (Mp*FER*) (aka Mp*THESEUS,* Mp*THE*) [44–46,56]. An Mp*fer/the* mutant was identified in a large T-DNA screen for defective rhizoid formation, developing short and irregularly shaped rhizoids with brown tips, indicating rhizoid rupture [56]. In the same screen, a mutant affecting the ortholog of the *A. thaliana* receptor-like cytoplasmic kinase *MARIS* (At*MRI*), known to act downstream of At*FER*, was identified with a similar phenotype (named Mp*mri* aka Mp*pti*, Mp7g17560 [Mapoly0051s0094]) [56,57]. As in *A. thaliana*, a dominant active version of Mp*MRI* can partially rescue the Mp*fer* rhizoid phenotype [57]. This suggests that at least some of the machinery associated with cell elongation and CWI sensing is conserved between *A. thaliana* and *M. polymorpha*.

Here, we report that *Cr*RLK1L function is required in a variety of aspects of *M. polymorpha* gametophyte development. Phylogenetic analyses suggest that *Cr*RLK1L genes first appeared in the common ancestor of land plants. The characterization of lines with reduced Mp*FER* levels indicates that, in addition to its function in rhizoid formation, Mp*FER* controls cell size and organ growth and is involved in male gametogenesis and fertility. Analysis of the Mp*FER* expression pattern points to an involvement in female sexual organogenesis and sporophyte development. Our data suggests that the broad involvement of *Cr*RLK1L function in the development and physiology of land plants is an ancestral and conserved characteristic, although the functions of *Cr*RLK1Ls were extended and adapted to control additional developmental processes in the sporophyte in the course of land plant evolution.

Results

*Cr*RLK1L is conserved in land plants and arose in this lineage

The *M. polymorpha* genome encodes a single *Cr*RLK1L homolog (Mp4g15890 [Mapoly0869s0001]) [44–46]. Like other *Cr*RLK1L members, this gene encodes an intracellular serine/threonine kinase domain, a transmembrane domain, and an extracellular malectin-like domain with two malectin domains (Figure 1A). Given that the ECD of *Cr*RLK1Ls in *A. thaliana* is crucial for their function and, in contrast to the kinase domain, not interchangeable [58], we performed a phylogenetic analysis with the amino acid sequences of the predicted malectin-like domain of Mp4g15890, the five members of the moss *Physcomitrella patens*, the two of the lycophyte *Selaginella moellendorffii*, and the 17 *Cr*RLK1Ls of *A. thaliana* (Figure 1B). The *M. polymorpha Cr*RLK1L member grouped together with the *Cr*RLK1Ls of basal land plants and was in the same clade as AtFER, while AtTHE1 was in a different one (Figure 1B). Based on this phylogenetic position and the fact that the malectin-like domain of the *M. polymorpha Cr*RLK1L shared the highest amino acid identity with AtFER (Figure S1A), we named it MpFER [45,46,57], but it is also known as MpTHE [56].

Interestingly, no significant similarity to the MpFER malectin-like domain was found when compared to available genomic data of six Chlorophyte algae (*Chlamydomonas reinhardtii, Dunaliella salina, Volvox carteri, Coccomyxa subellipsoidea, Micromonas pusilla*, *Ostreococcus lucimarinus*) and expression data of six Charophycean algae (*Klebsormidium nitens, Nitella mirabilis, Coleochaete orbicularis, Spirogyra pratensis, Mesostigma viride*, *Closterium peracerosum–strigosum–littorale* complex). In *Closterium* complex, an RK named CpRLK1 expressed during sexual reproduction was suggested to be a *Cr*RLK1L homolog [59]. However, comparing the full sequence or the ECD of CpRLK1 with the predicted *M. polymorpha* proteome, higher identity to another RK was

found (Figures S1B and S1C). Moreover, no RALF orthologs have been reported in algae, suggesting the origin of the *Cr*RLK1L pathway in land plants [45].

To further support MpFER as a member of the *Cr*RLK1L subfamily, the three-dimensional structure of its ECD was modelled [60] using the structure of the AtFER ECD (PDB 6a5b.1A, [35]) as a template (Figure 1C). Overall, the predicted structure of the MpFER ECD is highly similar to that of AtFER, keeping an almost identical number of secondary structures (7 alpha-helices and 33 beta-sheets in the MpFER ECD [35] and 8 alpha-helix and 34 beta-sheets in the AtFER ECD, respectively), and a similar spatial disposition for 32 of the beta-sheet structures and 6 of the alpha-helices (Figure 1C). When comparing the structural superposition of the AtFER and MpFER ECDs (Figures 1D and S1D), we observed that most conserved parts of the malectin-like domain are in the core of the protein, while the more variable parts are located peripherally. Moreover, the 3D structure of the CpRLK1 ECD could not be properly modelled using the AtFER ECD (Figures S1D and S1E). Taken together, these results suggest that the malectin-like domain of MpFER could interact with similar proteins as AtFER does in *A. thaliana*, and may thus be involved in similar pathways. Sequence comparison of the MpFER kinase domain showed a conservation of the activation loop and a Lys important for catalytic activity (Figure 1E). Furthermore, several determined phosphorylation sites found in AtFER, AtERU, and CrRLK1 were conserved in MpFER (Figure 1E) [13,33,61,62]. Thus, we propose MpFER to be basal and orthologous to all other land plant *Cr*RLK1Ls, and that the *Cr*RLK1L family arose as plants conquered land.

Mp*FER* is broadly expressed throughout the *M. polymorpha* life cycle

In *A. thaliana*, the expression patterns of the 17 *Cr*RLK1L members span vegetative and reproductive stages and both generations of the life cycle (reviewed in [43]), pointing to

the importance of *Cr*RLK1Ls for basic cellular functions. To assess whether this pattern is reflected in the land plant with the most ancestral characteristics, a promoter fragment of 3.2 kb (*pro*Mp*FER*) was used to drive expression of a triple yellow fluorescent protein (trpVNS) with a nuclear localization signal (*pro*Mp*FER*:*trpVNS*) and transformed into *M. polymorpha* sporelings. All transformants expressing the trpVNS fluorescent protein (45 of 48 independent lines) exhibited an indistinguishable expression pattern (Figure 2). During vegetative stages of gametophyte development, expression was observed in most cells of the thallus (Figure 2A). In concordance with the importance of Mp*FER* for rhizoids [56], high trpVNS expression was observed in these tip-growing cells (Figure 2B). While trpVNS was expressed in gemma cups, no expression was observed in mature gemmae, possibly due to their dormancy (Figure 2C).

In mature female sexual organs, strong expression was observed in the entire archegoniophore (Figure 2D). The archegonia expressed trpVNS in most cells, except for the egg cell (Figure 2E). However, after fertilization, proMp*FER*:*trpVNS* became active in the zygote (Figure 2F). Inside the sporogonium, the sporogenous cells and subsequently the developing spores, but not the elater cells, strongly expressed trpVNS (Figure 2I). In male sexual organs, trpVNS was broadly detected in the antheridial splash platform (Figure 2G) and, specifically, in the spermatogenous tissue of the antheridia and the non-reproductive jacket cells surrounding them at different developmental stages (Figure 2H). Taken together, Mp*FER* is expressed in most tissues during vegetative stages of gametophyte development as well as in the antheridia and archegonia during the sexual reproduction. Interestingly, the proMp*FER* promoter is not active in mature gemmae and the unfertilized, quiescent egg cell, although expression is initiated after dormancy and in the zygote. In concordance with the collectively ubiquitous expression of *Cr*RLK1Ls in *A.*

198 *thaliana*, the Mp*FER* expression pattern reinforces the importance of this family for basic
199 cellular functions in land plants.
200
201 **Mp*FER* controls cell expansion during vegetative gametophyte development**
202 To analyze the function of Mp*FER*, three independent artificial microRNA constructs
203 targeting Mp*FER* were designed (amiR-Mp*FER*), based on the endogenous microRNA
204 Mp*miR160* (Figure S2, [63]) and driven by the ubiquitous $_{pro}$Mp*EF1* promoter [64]. While
205 amiR-Mp*FER*1 and amiR-Mp*FER*2 target sites in the ECD coding sequence, amiR-
206 Mp*FER*3 targets the sequence encoding the kinase domain (Figures 3A and 3B). For
207 each amiR-Mp*FER* construct, several independent transgenic lines were obtained that
208 showed a reduction in thallus size (Figures 3C, 3D and S3A). Mp*FER* levels were
209 quantified by qRT-PCR in two independent amiR-Mp*FER*2 and amiR-Mp*FER*3 lines
210 each, which showed a similar phenotype (Figure 3E). Mp*FER* expression ranged from
211 10% to 20% of the wild-type level in all amiR-Mp*FER* lines analyzed (Figure 3E).
212 Previously, the T-DNA insertion mutant Mp*fer-1* was identified in a screen for mutants
213 with defective rhizoids ([56], referred to as Mp*the*). As the T-DNA inserted into the 3' UTR
214 of the Mp*FER* gene (Figure 3A; [56]), Mp*FER* expression was analyzed by qRT-PCR but
215 it showed no reduction compared to the wild type (Figure 3F), suggesting that the T-DNA
216 insertion does not affect Mp*FER* transcription. However, thallus size of Mp*fer-1* mutants
217 is similar to that of amiR-Mp*FER* lines (Figures 3C and 3D), suggesting that MpFER
218 function is partially affected by the T-DNA insertion.
219 Rhizoids are tip-growing cells analogous to the root hairs in flowering plants
220 (angiosperms). Reduced Mp*FER* activity strongly impaired rhizoid formation and the
221 rhizoids collapsed (Figure 3C). This had also been reported for the Mp*fer-1* mutant [56]
222 and is in concordance with the function of At*FER* and At*ANX1/2* in tip-growing root hairs

[12,16,33,65] and pollen tubes [8,14], respectively. As *Cr*RLK1L members are important for cell expansion in angiosperms [7,9,11,19,34,66,67], cell size of epidermal thallus cells in fully differentiated regions with minimal growth was measured in Mp*fer-1* and amiR-Mp*FER* lines, showing a reduction in cell area as compared to the wild type (Figures 3G, S3B and S3C). Although amiR-Mp*FER* lines produced more intact rhizoids than Mp*fer-1* mutants (Figure 3C), the average epidermal cell area was similarly reduced, although the distribution of cell areas differed between amiR-Mp*FER* lines and Mp*fer-1* (Figures 3G, S3B and S3C).

In conclusion, Mp*FER* has a fundamental role in rhizoid formation and growth during vegetative development. These results suggest an ancestral and conserved function of the *Cr*RLK1Ls in polar cell growth and cell expansion.

Mp*FER* is important for the morphological integrity of the gametophyte

Given that Mp*fer-1* and amiR-Mp*FER* lines retain some MpFER activity, we generated Mp*fer* knock-out mutants with the goal to unveil potentially hidden *Cr*RLK1L functions by generating a plant without any *Cr*RLK1L activity. Using CRISPR/Cas9, two sites in the ECD-coding sequence of Mp*FER* were targeted (Figure 4A). At least 10 independent lines were selected and analyzed for each target site. All plants with severely affected thallus development contained a frame shift mutation at the respective target site (Figures 4A-4C) while Mp*FER* was not affected in transgenic plants with normal development.

The thallus area of the newly generated, amorphic knock-out mutants was more strongly reduced compared to Mp*fer-1* [56], confirming that, like the amiR-Mp*FER* lines, Mp*fer-1* is a hypomorphic mutant (Figures 4C and 4D). In contrast, rhizoid integrity was similarly affected in hypo- and amorphic Mp*fer* alleles, suggesting that rhizoid formation is more sensitive to reduced Mp*FER* activity than thallus growth (Figures 4E-4F). Despite of the

248 strong impact on thallus development, both hypo- and amorphic Mp*fer* mutants form
249 gemma cups.
250 The strong disruption of thallus growth in amorphic Mp*fer* mutants prompted us to
251 investigate whether cells of the thallus died in the absence of Mp*FER* activity. Indeed,
252 using tryphan blue staining, we detected dead cells in these mutants, indicating a loss of
253 morphological integrity (Figure 4G).
254
255 **Some reproductive but not all CWI sensing functions of *Cr*RLK1Ls are conserved**
256 **in land plants**
257 In *A. thaliana*, at least seven *Cr*RLK1L family members play a role in reproduction, with
258 At*ANX1/2* and At*BUPS1/2* being important for pollen tube growth [8,14,18,32] and
259 At*FER*, At*HERK1*, and At*ANJ* for pollen tube reception by the synergid cells [6,17]. To
260 characterize the function of Mp*FER* in reproductive development, amiR-Mp*FER*3-2 lines
261 were transferred to sexual organ-inducing conditions [68]. The number of
262 antheridiophores produced was significantly less in amiR-Mp*FER* lines compared to the
263 wild type (Figures 5A and S3D) and the antheridiophore splash platforms were also
264 smaller (Figure 5B). The reduction in Mp*FER* expression in antheridiophores of amiR-
265 Mp*FER* lines was confirmed by qRT-PCR and results were comparable to those using
266 thallus tissue (Figure 5C). A pronounced reduction in spermatogenous tissue was
267 observed in many antheridia isolated from amiR-Mp*FER*3-2 lines (Figures 5D and 5E).
268 However, although the plants were grown under optimal conditions in axenic culture
269 boxes, the effects on reproductive structures could be partly indirect due to the reduction
270 in plant size and/or rhizoid function.
271 To determine male fertility of these amiR-Mp*FER* lines with reduced spermatogenous
272 tissue, we performed crosses with wild-type female plants. The spermatocyte

concentration harvested from wild-type antheridia was almost 3-fold higher than from amiR-Mp*FER* lines and was adjusted using a hemocytometer. In just one of the crosses (n=20), a single sporophyte was formed, resulting in 0.05 ± 0.05 (mean ± SE) sporophytes per archegoniophore, whereas the same females crossed with wild-type males yielded 9.95 ± 2.33 (mean ± SE) sporophytes per archegoniophore. In summary, Mp*FER* plays a role in antheridiophore development and spermatocytes of plants with reduced Mp*FER* activity are poorly fertile. Thus, *Cr*RLK1Ls have a conserved role in reproduction in addition to their role in cell expansion and integrity during vegetative development.

Some *A. thaliana Cr*RLK1Ls are involved in surveying CWI and in inhibiting growth when CWI is impaired. Cell wall defects caused either by mutations affecting cellulose biosynthesis or by treatment with isoxaben, a cellulose synthesis inhibitor, can be suppressed by a mutation in At*THE1* [7,28]. To investigate whether Mp*FER* also acts as CWI sensor, we treated wild-type, Mp*fer*, and amiR-Mp*FER*3-2 gemmae with isoxaben (Figure 5F). As in the wild type, isoxaben affected the development of gemmae with reduced Mp*FER* activity, all growing progressively less with increasing isoxaben concentration (Figure 5F). These results suggest that the function of At*THE1* in repressing cellular growth when CWI is impaired appeared later in the course of land plant evolution or was lost in the *Marchantia* lineage.

The *Cr*RLK1L signaling pathway is conserved in land plants

As downregulation of Mp*FER* or At*FER* produce similar phenotypes concerning polarized growth and cell expansion in *M. polymorpha* and *A. thaliana*, respectively, interspecific complementation was attempted. First, the coding sequence of Mp*FER* fused to the Green Fluorescent Protein (GFP) gene under the control of the viral *35S* promoter ($_{pro}$*35S*:Mp*FER-GFP*) was transformed into heterozygous At*fer-2* mutants. Then, GFP

298 expression at the cell periphery and complementation of the bursting root hair and
299 reduced rosette size phenotypes were assessed in transgenic plants (Figure 6A). At*fer-2*
300 homozygotes expressing the MpFER-GFP protein look similar to At*fer-2* mutants,
301 indicating that Mp*FER* does not complement these At*fer-2* loss-of-function phenotypes
302 (Figure 6A). In a complementary experiment, the coding sequence of At*FER* fused to the
303 Citrine gene under the control of the Mp*EF1* promoter ($_{pro}$Mp*EF1:*At*FER-Cit*) was
304 transformed into amiR-Mp*FER*3-2 plants. Ten independent lines with Citrine expression
305 at the cell periphery were phenotypically characterized (Figures 6B and 6C). All had
306 bursting rhizoids and a reduced thallus size, similar to the parental amiR-Mp*FER*3-2 line,
307 suggesting that At*FER* does not rescue the vegetative phenotypes produced by down-
308 regulation of Mp*FER*.
309 In *A. thaliana*, it was shown that AtFER forms a complex with AtRALF peptides and the
310 LRE/LLG co-receptors [35]. As no interspecific complementation was observed, the
311 conservation of binding surfaces between *Cr*RLK1L, RALF, and LRE homologs were
312 analyzed. The *M. polymorpha* genome encodes three RALF peptides (MpRALF:
313 Mp1g27120 [Mapoly0002s0166]; MpRALF2: Mp2g21670 [Mapoly0040s0047];
314 MpRALF3: Mp7g07270 [Mapoly0076s0067]) [44,45]. We performed a phylogenetic
315 analysis using the amino acid sequences of the predicted mature peptides of *A. thaliana*
316 and *M. polymorpha* RALFs (Figure S4A). All MpRALF peptides clustered together with
317 AtRALFs known to interact with *Cr*RLK1L receptors, including AtRALF1 and AtRALF23,
318 which serve as AtFER ligands [22,33] (Figure S4A). The MpRALFs shared the four
319 conserved Cys residues as well as the YXXY and YY motifs with the AtRALF1 subgroup
320 (Figure S4B). However, only MpRALF1 and MpRALF3 had an RRXL motif important for
321 S1P cleavage (Figures S4B and S4C)[69], consistent with the presence of one S1P
322 ortholog in basal plants (Mp8g07990 [Mapoly0155s0018], Figure S4D). There are two

MpLRE/LLG proteins encoded in the *M. polymorpha,* genome (Figure S5A). Both the MpLRE1 (Mp5g09600 [Mapoly0048s0110]) and MpLRE2 (Mp4g22100 [Mapoly0090s0020]) proteins showed conservation of the eight Cys and the ND motif distinctive of the family (Figure S5B); however, MpLRE1 did not contain a GPI anchoring site (Figure S5B). Structure prediction using AtLLG2 as a template [35] showed a conserved general structure (Figures S5C and S5D). Some of the Mp*RALF* and Mp*LRE* family members show a similar expression pattern as Mp*FER* (Figure S5F), suggesting that the corresponding proteins could form a complex similar to that described in *A. thaliana*.

To gain insights into the formation of a putative *Cr*RLK1L signaling complex, the MpFER/MpRALF/MpLRE complex was modelled. The general structure appeared conserved (Figure S5E); however, analysis of conserved sites between *M. polymorpha* and *A. thaliana* showed a low amino acid conservation in the interacting surfaces of the complex subunits (Figure 6D). This suggests that the lack of interspecific complementation may be due to differences in amino acids that are important for complex formation, and that the proteins forming the complex have diverged, following distinct routes of co-evolution in the two lineages.

Because interspecific complementation of the amiR-Mp*FER* phenotypes was unsuccessful, we asked whether suppression using a downstream component of *Cr*RLK1L signaling identified in *A. thaliana* was possible. AtMRI, a receptor-like cytoplasmic kinase, acts downstream of At*FER* or At*ANX1/2* in the regulation of polar tip growth [70,71]. The dominant AtMRI^{R240C} mutation can suppress pollen tube rupture in the At*anx1*/At*anx2* double mutant and the root hair defects of At*fer-4* [70,71]. A mutation in Mp*MRI* (aka Mp*PTI*) with a similar bursting rhizoid phenotype as observed in Mp*fer-1*, was identified in the same genetic screen for *M. polymorpha* mutants with defective

rhizoids [56]. To test whether Mp*MRI* is a conserved downstream component of the Mp*FER* signal transduction pathway, a dominant-active form of the protein equivalent to AtMRI^{R240C} was transformed into the amiR-Mp*FER*3-2 line, driven by 2 kb of the endogenous promoter ($_{pro}$Mp*MRI:*Mp*MRI*^{R240C}). Several independent lines showed a partial restoration of rhizoid growth; however, we also observed defects in thallus development of lines with higher levels of Mp*MRI* expression, mainly abnormalities in the epidermis (Figures 6E and S6A-S6E). This suggest that Mp*MRI* acts downstream of Mp*FER* in the signal transduction pathway controlling polarized growth since the origin of land plants, in agreement with a recent report on the functional characterization of Mp*MRI* [57].

Overexpression of Mp*FER* affects morphological integrity

Because overexpressing At*FER* in *M. polymorpha* did neither lead to any obvious phenotypes nor complementation of amiR-Mp*FER* lines (Figures 6B and 6C), we also overexpressed At*FER* and Mp*FER* in the wild type. As in the amiR-Mp*FER* background, overexpression of AtFER ($_{pro}$Mp*EF1:*At*FER-Cit*) in a wild-type background had no effect, consistent with the idea that At*FER* is unable to form a complex with the corresponding *M. polymorpha* proteins. However, when expressing an MpFER-Citrine fusion protein ($_{pro}$Mp*EF1:*Mp*FER-Cit*) in wild-type plants, thallus development was strongly affected (Figure 7A). As expected, MpFER-Cit localized to the membrane (Figure 7B), and higher protein levels correlated with more severe phenotype (Figures 7A and 7C). Scanning electron microscopy of epidermis of plant expressing high levels of Mp*FER* showed defects in the formation of air chambers and air pores (Figure 7D), similar to what we observed when expressing the dominant-active Mp*MRI*^{R240C} (Figure S6A-S6C). Moreover, overexpression of MpFER affects the number of lobes in the antheridial

receptacle, producing only 4 instead of 8 (Figure S6F), supporting the importance of MpFER during sexual development. Considering the importance of Mp*FER* for normal rhizoid formation, we also analyzed rhizoids in the $_{pro}$Mp*EF1:*Mp*FER-Cit* lines: while rhizoid morphology looked normal, a decrease in rhizoid number was observed (Figures 7E and 7F).

Taken together, the results obtained by overexpressing Mp*FER* support the role of Mp*FER* in cell expansion and maintaining tissue integrity during plant morphogenesis.

Discussion

During land plant evolution, many developmental aspects have changed in order to adapt to new environments, producing the enormous diversity observed in the plant kingdom. However, the control and maintenance of CWI remained a key aspect for the biology of a plant cell. CWI sensing is not only important for vegetative growth by cell expansion, but it is also essential for sexual reproduction and defense responses.

The *Cr*RLK1L family was first characterized for its importance during angiosperm fertilization, a process comprising aspects of polar cell elongation, CWI control, and cell-cell communication [6,30,31]. Lately, different members of this family were found to carry out diametrically opposite roles in diverse aspects of plant development, which has made it difficult to define the core or ancestral function of this gene family comprising 17-members in *A. thaliana* [6–12,14–20,32].

Here, we report the characterization of the single *Cr*RLK1L gene encoded in the genome of *M. polymorpha*. Structurally, the MpFER ECD and kinase domain share similarities with previous characterized *Cr*RLK1L members, including the malectin-like domain and conserved phosphorylation sites. Conservation of RALF and LRE members in *M. polymorpha* suggests that MpFER also forms a complex at the plasma membrane [35].

While modeling predicted that the general structure of the complex was conserved, the interaction surfaces seem to have diverged and co-evolved independently in the respective lineages.

We observed a broad involvement of Mp*FER* at both vegetative and reproductive stages of development: During vegetative growth of the gametophyte, Mp*FER* is required for rhizoid formation and cell expansion but it also plays a role in male gametogenesis and is expressed in female reproductive organs. These findings suggest that the *Cr*RLK1Ls have, also in ancestral land plants, held roles in various aspects of both vegetative and reproductive development. Thus, the role of *Cr*RLK1Ls in angiosperm reproduction does not represent a derived feature from a purely vegetative function in cell elongation in bryophytes, but constitutes a conserved feature of this gene family.

Moreover, the almost ubiquitous expression of Mp*FER* in *M. polymorpha* is consistent with the collective expression of different *Cr*RLK1L members in essentially all tissues and organs of *A. thaliana* [43]. Thus, gene duplication allowed the expansion of the *Cr*RLK1L family in angiosperms, diversifying their expression patterns and functions but also leading to genetic redundancy [8,17,32,43].

*Cr*RLK1L members are important sensors of CWI during polarized growth, both in pollen tubes [8,32] and root hairs [16]. In early divergent land plants, rhizoids are tip-growing cell with a function analogous to that of root hairs, important for taking up nutrients and water [56,72]. Based on the conservation of many genes controlling the development and growth of tip-growing cells forming rooting systems, it was suggested that these pathways were active in the earliest land plants that existed about 470 million years ago [56]. That Mp*FER* also controls rhizoid integrity points to the importance of the *Cr*RLK1L pathway for polarized growth since the origin of land plants. Moreover, the fact that amorphic Mp*fer* mutants contain many dead cells demonstrates the importance of the *Cr*RLK1L pathway

for cellular integrity during vegetative growth. This aspect has not yet been reported for *A. thaliana Cr*RLK1L mutants, possibly due to genetic redundancy among family members.

The signaling mechanisms downstream of Mp*FER* in *M. polymorpha* development are still unclear. Mp*MRI*, the *M. polymorpha* ortholog of At*MRI*, which acts downstream of AtFER and AtANX1/2 in *A. thaliana* during polarized growth [70], does have a similar rhizoid phenotype as Mp*FER* [56,57]. The suppression of the rhizoid phenotype in amiR-Mp*FER* transformants with the constitutively active form MpMRI^{R240C} corroborates a conserved *Cr*RLK1L signaling cascade during polarized growth in *M. polymorpha* but whether this pathway also relies on Ca^{2+} and reactive oxygen species (ROS) as second messengers as it does in *A. thaliana* remains to be determined.

In *A. thaliana*, loss-of-function mutations in the motor protein AtKINESIN-13a, a microtubule-based motor, cause cell elongation in petals, leaves, and hypocotyls concomitant with changes in cell wall composition in leaves [73]. This effect depends on functional AtTHE1 and does not occur in At*kinesin-13-a/*At*the1* double mutants. Interestingly, in this case, AtTHE1 stimulates cell elongation in response to defects in cell wall deposition [73]. Based on our results, we have no indication that Mp*FER* acts as a CWI sensor and regulates growth similar to At*THE1* in response to cell wall disturbances. We have not observed a context in *M. polymorpha* development in which Mp*FER* inhibits cell expansion. Therefore, the ability to restrict growth in response to disturbances in CWI could represent an evolutionary derived feature, as gene duplication allowed for the diversification and specialization of *Cr*RLK1Ls to regulate cellular growth in a more complex and context-dependent way. The capacity to flexibly regulate growth appears to be fundamentally context-dependent, as a similar discrepancy in promoting or inhibiting growth is also known for some well-studied growth promoting agents, like the

448 phytohormones auxin and brassinosteroid, which can have growth-inhibitory effects
449 dependent on tissue and concentration. The reverse was noted for the phytohormones
450 ethylene and abscisic acid, which are usually considered growth inhibitors but can also
451 promote growth, dependent on the context [74–76].
452 Taken together, our results suggest an ancestral and conserved function of the *Cr*RLK1Ls
453 in polar cell growth and cell expansion, but also during sexual reproduction. In addition,
454 we probe the relevance of *Cr*RLK1L members for cell integrity and morphogenesis. In
455 angiosperms, *Cr*RLK1Ls occupy an important position at the interface of developmental
456 and environmental inputs, which are integrated by a downstream signaling machinery
457 that controls cell shape and polar growth to ensure normal development, *e.g.* by
458 preventing cell rupture upon CWI defects. Whether the same downstream machinery is
459 utilized in a similar fashion in *M. polymorpha* remains to be shown, even though the
460 similarity in function points to a related mechanism. Even less is known about upstream
461 aspects of *Cr*RLK1L signaling. Future studies on the transcriptional regulation and the
462 upstream components, such as the putative RALF ligand(s), in the highly simplified *M.*
463 *polymorpha* system could provide fundamental insights into the molecular mechanism of
464 the *Cr*RLK1L pathway, which is so central to land plant physiology, growth, and
465 development.
466

467 ## Acknowledgments

468 We thank Liam Dolan for kindly providing the Mp*fer-1*/Mp*the* mutant, Valeria Gagliardini
469 for help with qRT-PCR and ddPCR, Anja Grossniklaus for help in measuring epidermal
470 cell area, Célia Baroux and Ethel Mendocillo-Sato for instructions on confocal microscopy
471 and the use of Imaris Software, Isabel Monte and Cyril Zipfel for comments on the

manuscript, and Christof Eichenberger, Frédérique Pasquer, Arturo Bolaños, Daniela Guthörl, Daniel Prata, and Peter Kopf for general lab support.

Author contributions

MAM: Conceptualization, Formal analysis, Investigation, Methodology, Validation, Visualization, Writing – original draft, Writing – review & editing

MR: Conceptualization, Formal analysis, Investigation, Methodology, Validation, Visualization, Funding acquisition, Writing – original draft, Writing – review & editing

AF-G: Data curation, Formal analysis, Software, Validation, Visualization, Writing – original draft, Writing – review & editing

DM: Formal analysis, Investigation, Validation, Writing – review & editing

PG: Formal analysis, Investigation, Validation, Writing – review & editing

JLB: Funding acquisition, Resources, Supervision, Validation, Writing – review & editing

UG: Conceptualization, Formal analysis, Funding acquisition, Project administration, Supervision, Validation, Writing – original draft, Writing – review & editing

Funding disclosure

This work was supported by the University of Zurich, Monash University, and grants from the Forschungskredit of the University of Zurich (http://www.research.uzh.ch/en/funding/phd/fkcandoc; FK-16-090) to MR, the Australian Research Council (http://www.arc.gov.au; DP130100177) to JLB, and the Swiss National Science Foundation (http://www.snf.ch; 310030B_160336 and 31003A_179553) to UG. The funders had no role in study design, data collection and analysis, decision to publish, or preparation of the manuscript.

Competing interests

The authors have declared that no competing interests exist.

Main figure titles and legends

Figure 1. *Cr*RLK1Ls Are Conserved among Land Plants

(A) Representation of AtFER and MpFER proteins. Malectin-like domains are represented in blue and kinase domains in green. SP, signal peptide; TM, transmembrane domain (yellow). Amino acids important for regulation and activity are marked in red, violet, and light blue as described in Figure 1E.

(B) A rooted neighbor-joining tree of the amino acid sequence of the predicted malectin-like domain. *Cr*RLK1L members from *Marchantia polymorpha* (Mp), *Physcomitrella patens* (Pp), *Selaginella moellendorffii* (Smo), and *Arabidopsis thaliana* (At) were used. The numbers indicate the bootstrap values (%) from 1000 replications. The given scale represents a substitution frequency of 0.1 amino acids per site.

(C) Cartoon representation of the predicted three-dimensional structure of the MpFER malectin-like domain, showing predicted alpha-helix and beta-sheet structures.

(D) Structural superposition of the malectin-like domains of AtFER (blue) and MpFER (green).

(E) Alignment of the cytoplasmic domains of MpFER, AtERU, AtFER, and *Cr*RLK. Kinase domains are in green, putative phosphorylation sites in light blue (Ser) and violet (Thr), and the conserved catalytic Lys in red.

See also Figure S1

Figure 2. Mp*FER* Is Broadly Expressed in most Tissues throughout the *M. polymorpha* Life Cycle

Expression of $_{pro}$Mp*FER*:*trpVNS* in different organs of male and female *M. polymorpha* plants. Fluorescence is visualized as either green (epifluorescence microscope) or yellow (confocal microscope) color, depending on the panel.

(A to D) Bright field (left) and epifluorescence (right) images of a thallus, (A) rhizoid (C), gemmae cups (C), and an archegoniophore (D). Red arrows indicate meristematic zones, the yellow arrow gemmae. Scale bars, 0.5 mm.

(E and F) Confocal images of archegonia before (E) and 2 days after fertilization (F). Scale bar, 50 µm.

(G) Bright field (left) and epifluorescence (right) images of an antheridiophore. Scale bar, 1 mm.

(H) Confocal image of antheridia. Scale bar, 100 µm.

(I) Confocal image of sporophyte and spores. Scale bar, 25µm.

Figure 3. Mp*FER* Controls Cell Size during Gametophyte Development

(A) Representation of the mature Mp*FER* mRNA. Coding sequence are in green, locations of the amiRNA target sites in blue.

(B) Base complementary between mature amiR-Mp*FER*1, amiR-Mp*FER*2, and amiR-Mp*FER*3 with the Mp*FER* transcript.

(C) Relative expression level of Mp*FER* in thallus tissue from wild-type (WT; Tak1) and two independent insertion lines of amiR-Mp*FER*2 and amiR-Mp*FER*3, as measured by qRT-PCR. Mp*EF1* was used as internal control. Shown are means ± standard errors of the means (SEM) of three biological replicates. *P < 0.01, one-way analysis of variance (ANOVA).

(D) Relative expression level of Mp*FER* in WT and Mp*fer-1* thallus tissue, as measured by qRT-PCR. Mp*EF1* was used as internal control. Shown are means ± SEM of three biological replicates. *P < 0.01, one-way ANOVA.

(E) Representative pictures of 10-day old gemmalings of WT, Mp*fer-1*, and amiR-Mp*FER*3-2 lines. Scale bar, 1 mm.

(F) Thallus area of WT, Mp*fer-1*, and amiR-Mp*FER*3-2 lines. n = 30, outliers are indicated as black dots.

(G) Violin plot of cell size in WT, *Mpfer-1*, and amiR-Mp*FER*3-2 lines. Significant differences are indicated according to the non-parametric Kruskal-Wallis test and linear regression models (***p<0.001).

See also Figures S2 and S3

Figure 4. The Integrity of Thalli from Mp*fer* Knock-out Lines Is Severely Affected

(A) Representation of the mature Mp*FER* mRNA with the coding sequence in green, and the location of the gRNA target sites in red.

(B) Sequences of gRNA target sites in the confirmed Mp*fer* knock-out mutants. Deletions and insertions are highlighted in red.

(C) Representative pictures of 10-day old gemmalings of WT, Mp*fer-1*, and two independent Mp*fer* knock-out mutants. Scale bar, 0.5 cm.

(D) Thallus area of 10-day old gemmalings of WT, Mp*fer-1*, and two independent Mp*fer* knock-out mutants. n = 30.

(E) Representative pictures of 3-day old gemmalings growing in upside-down plates of WT, Mp*fer-1*, and two independent Mp*fer* knock-out mutants. Scale bar, 500 µm.

(F) Rhizoid number in 3-day old gemmalings of WT, Mp*fer-1*, and two independent Mp*fer* knock-out mutants. n = 30.

(G) Trypan blue staining of 7-days old gemmalings of WT, Mp*fer-1*, and two independent Mp*fer* knock-out mutants. Scale bar, 1 mm.

Figure 5. Conservation of *Cr*RLK1L Function in Land Plants

(A) Number of antheridiophores produced per plant for wild-type (WT, n=9) and two independent amiR-Mp*FER*3 lines (amiR-Mp*FER*3-2, n = 9; amiR-Mp*FER*3-3, n = 12). Shown are means ± SEM of two biological replicates. Means with same letter do not differ significant different with P > 0.05, one-way ANOVA, Duncan test.

(B) Antheridiophore splash platform size distribution of WT (n = 32), amiR-Mp*FER*2-3 (n = 34), and amiR-Mp*FER*3-3 (n = 11) lines. For all antheridia with a stalk >8 mm, length and width of the platform were recorded.

(C) qRT-PCR of Mp*FER* levels in antheridiophores in a WT and amiR-Mp*FER*3-3 line. Mp*EF1* was used as internal control. Shown are means ± SEM of three biological replicates. *P < 0.01, ANOVA.

(D and E) Mature antheridia of a WT (D) and amiR-Mp*FER*3-3 line (E). Bright field images (left) and in cross-section (right). The spermatogenous areas are indicated in red. Scale bar, 100μm.

(F) Thallus area of 15-day old gemmalings of WT, *Mpfer-1* mutant, and an amiR-Mp*FER*3-2 line growing on media containing different isoxaben concentrations (nM). n = 30, outliers are indicated as black dots. Shown are means ± SEM of two biological replicates. Means designated by the same letter do not significantly differ at P > 0.05, one-way ANOVA, Duncan test.

See also Figure S3

Figure 6. Interspecific Complementation of *A. thaliana* and *M. polymorpha* Plants with Reduced Levels of *FER* Activity

(A) Roots of independent *A. thaliana* lines expressing 35S:Mp*FER-GFP* in L*er* wild-type (WT) and At*fer-2* plants. Scale bar, 200 µm.

(B) 10-day old gemmalings of WT and amiR-Mp*FER*3-2 *M. polymorpha* plants with and without expression of At*FER-Cit*. Scale bar, 0.5 mm.

(C) Citrine expression in 7-day old gemmalings of WT and amiR-Mp*FER*3-2 plants with and without expression of At*FER-Cit*. Scale bar, 100 µm.

(D) Cartoon representation of the structural conservation of the *Cr*RLK1L^{ECD}/LRE/RALF complex by comparing AtFER/MpFER and AtLLG2/MpLRE1. Blue and green represent spatially highly conserved regions of *Cr*RLK1L and LRE homologs, respectively. Red indicates structural regions with low spatial conservation, lilac the C-terminal part of AtRALF23, and black arrows the interaction regions of the three proteins.

(E) Complementation of amiR-Mp*FER* lines with a dominant-active version of Mp*MRI* under its own promoter ($_{pro}$Mp*MRI*:*MRI*^{R240C}). Scale bar, 1 mm.

See also Figures S4-S7

Figure 7: Overexpression of Mp*FER* Affects Morphological Integrity

(A) Representative pictures of 10-day old gemmalings of wild-type (WT, Tak1) and different lines overexpressing Mp*FER* ($_{pro}$Mp*EF1:*Mp*FER-Cit)*. Scale bar, 1 mm.

(B) Citrine expression at the plasma membrane in WT and $_{pro}$Mp*EF1:*Mp*FER-Cit* lines *#5* and #9 as observed under confocal microscopy. Scale bar, 20 µm.

(C) Western blot analysis of $_{pro}$Mp*EF1:*Mp*FER-Cit* lines using an anti-GFP antibody. $_{pro}$Mp*EF1:Cit* and WT lines were used as positive and negative controls, respectively. The

618 Ponceau membrane staining of the most intense band at 55 kDa (presumably Rubisco)
619 was used as a loading control.
620 (D) Scanning electron microscopical images of thalli from 20-day old plants of WT and
621 $_{pro}$Mp*EF1:*Mp*FER-Cit* lines *#5* and #9. Scale bar, 500 µm.
622 (E) Representative pictures of 3-day old gemmalings growing in upside-down plates of
623 WT and $_{pro}$Mp*EF1:*Mp*FER-Cit* lines *#5* and #9. Scale bar, 1 mm.
624 (F) Number of rhizoids in 3-day old gemmalings of WT and $_{pro}$Mp*EF1:*Mp*FER-Cit* lines *#5*
625 and #9. n = 30.
626 See also Figure S6
627

628 Supplemental figure titles and legends

629

630 **Figure S1. The *Cr*RLK1L Family Appeared together with Land Plants. Related to**
631 **Figure 1.**
632 (A) Percentage of identity of the malectin-like domain, the complete ECD, and the full
633 protein of MpFER with AtFER, AtANX1, AtANX2, and AtTHE1.
634 (B) Percentage of identity of the ECD and full protein of CpRLK1 with MpFER, AtFER,
635 and Mapoly001s0111.
636 (C) A rooted neighbor-joining tree of the amino acid sequence of the predicted malectin-
637 like domain was generated using ClustalW. *Cr*RLK1L members from *Marchantia*
638 *polymorpha* (Mp), *Physcomitrella patens* (Pp), *Selaginella moellendorffii* (Smoe), and
639 *Arabidopsis thaliana* (At) were used. Algal CpRLK1 and Mapoly001s0111 were also
640 included. The numbers indicate the bootstrap values (%) from 1000 replications. The
641 given scale represents a substitution frequency of 0.1 amino acids per site.

(D) Qmean value for prediction of MpFER or CpRLK1 3D structures of the ECD based on the AtFER ECD. Green numbers indicate a good modelling fit, red numbers indicates a bad modelling fit.

(E) Structural superposition of the ECD of AtFER (blue) and CpRLK1 (purple).

Figure S2. Design of amiR-Mp*FER* Precursors. Related to Figure 3.

(A) Mp*miR160* (Mapoly0002s0211, Mp1g26670) and amiR-Mp*FER*1, amiR-Mp*FER*2, and amiR-Mp*FER* sequences. miRNA sequences are in red and miRNA* in blue. Cloning sequences from amiR-Mp*FER* constructs are in bold.

(B) Drawing of the minimum free energy structure of Mp*miR160* and amiR-Mp*FER*3 constructs predicted by the RNAfold web server (http://rna.tbi.univie.ac.at//cgi-bin/RNAWebSuite/RNAfold.cgi). Red arrows indicate location and orientation of the mature miRNA in the precursor. The structures are colored by base-pairing probabilities; for unpaired regions the color denotes the probability of being unpaired.

Figure S3. Reduction in Thallus and Cell Area in Plants with Reduced Mp*FER* Levels. Related to Figures 3 and 5.

(A) Thallus area of wild-type (WT), Mp*fer-1*, and amiR-Mp*FER*3-2 plants at different days after putting gemmae on plates. n = 30, outliers are indicated as black dots. Areas were estimated using ImageJ software.

(B) Representative images from cell surface areas measured in WT, amiR-Mp*FER*2-1, and amiR-Mp*FER*3-2 plants. Scale bar, 50 μm.

(C) Difference in cell size between WT, amiR-Mp*FER*2-1, *and* amiR-Mp*FER*3-2 plants is significant ($p<0.001$) based on the nonparametric Kruskal-Wallis test and a linear regression model with a highly significant interaction ($p<0.001$).

(D) Induction of antheridiophores in WT and two independent amiR-Mp*FER*3 lines. Three plants were grown in each sterile plastic box under far-red light induction.

Figure S4. MpRALF Peptides Belong to the AtRALF1-clade of the RALF Family. Related to Figure 6.

(A) A rooted neighbor-joining tree of the amino acid sequence of the predicted mature RALF peptides was generated using ClustalW. RALF members from *M. polymorpha* and *A. thaliana* were used. Red arrows indicate RALFs that are known ligands of *Cr*RLK1Ls. The numbers indicate the bootstrap values (%) from 1000 replications. The given scale represents a substitution frequency of 0.1 amino acids per site.

(B) Amino acid sequence comparison of AtRALF1 and MpRALF1-3. Predicted signal peptides are in black, predicted mature peptides in light blue, conserved Cys in red, and predicted S1P recognition sites in violet.

(C) Processing pathway AtRALF1 by the S1P protease.

(D) A rooted neighbor-joining tree of the amino acid sequence of the S1P orthologs was generated using ClustalW. S1P members from *M. polymorpha*, *P. patens*, and *A. thaliana* were used. The numbers indicate the bootstrap values (%) from 1000 replications. The given scale represents a substitution frequency of 0.1 amino acids per site.

Figure S5. Two LORELEI-like Proteins Are Encoded in the *M. polymorpha* Genome. Related to Figure 6.

(A) A rooted neighbor-joining tree of the amino acid sequence of LRE orthologs was generated using ClustalW. LRE members from *M. polymorpha*, *P. patens*, and *A. thaliana* were used. The numbers indicate the bootstrap values (%) from 1000 replications. The given scale represents a substitution frequency of 0.1 amino acids per site.

692 (B) Amino acid sequence of AtLRE, MpLRE1, and MpLRE2. Conserved Cys are in light
693 blue, the ND motif in red, and the GPI-anchoring site in green.
694 (C) Cartoon representation of the predicted 3-dimensional structure of MpLRE1, showing
695 predicted alpha-helices.
696 (D) Structural superposition of AtLGG2 (blue) and MpLRE1 (green).
697 (E) Cartoon representation of the predicted 3-dimensional structure of the
698 MpFER/MpLRE1/MpRALF1 complex, showing predicted alpha-helices and beta-sheets.
699 (F) Heatmap depicting relative gene expression based on RNAseq data (row-Z-score of
700 vs normalized counts) of Mp*FER* and the *M. polymorpha* orthologs of At*MRI*, At*RALF1*,
701 and At*LRE* across different tissues. Vegetative and reproductive tissues are grouped by
702 green and orange, respectively. Averaged expression values are represented with colors
703 of increasing red and blue intensity indicating upregulation and downregulation of gene
704 expression, respectively.
705
706 **Figure S6. Expression of Mp*MRI*^{R240C} Suppresses the Bursted Rhizoid Phenotype**
707 **of amiR-Mp*FER*3 Lines but Leads to Aberrant Epidermis Development. Related to**
708 **Figures 6 and 7.**
709 (A to C) Epidemical pictures of thalli from the wild-type (WT, Tak-1) (A), and amiR-
710 Mp*FER*3 + $_{pro}$MpMRI:Mp*MRI*^{R240C} lines #6 (B) and #8 (C), which both partially suppressed
711 the bursting rhizoid phenotype (Fig. 6).
712 (D and E) Relative expression of Mp*FER* (D) and Mp*MRI* (E) against the geometric mean
713 of the reference genes Mp*ACT1*, Mp*ACT7*, and Mp*APT3* in WT, amiR-Mp*FER*3-2, and 5
714 lines (#5 to #9) co-transformed with the amiR-Mp*FER*3-2 and $_{pro}$MpMRI:Mp*MRI*^{R240C}
715 constructs. Expression levels of three biological replicates were assessed by droplet
716 digital PCR (ddPCR). The y-axis corresponds to the log2-ratio between the test and the

717 geometric mean of the reference genes. Shown are means ± SEMs of three biological
718 replicates. *P < 0.01, one-way ANOVA.
719 (F) Representative images of the antheridial receptacle of WT and $_{pro}$Mp*EF1:*Mp*FER-Cit*
720 plants. Scale bar, 2 mm.
721
722 **Figure S7. Structure Assessment and Quality Estimations of the MpFER and**
723 **MpLRE 3-dimensional Models. Related to Figure 6.**
724 QMEAN score barplot indicating quality estimates of the predicted models, across their
725 aminoacidic sequence. Below the barplots, the corresponding secondary structures are
726 displayed for both target and template sequences, with alpha-helixes represented by light
727 purple boxes and beta-sheets by green arrows. All plots were adapted from the model
728 report produced by the SWISS-MODEL workspace.
729 (A) MpFER^{ECD}, for which AtFER was used as a template (PDB 6a5b.1A).
730 (B) MpLRE1, for which AtLLG2 was used as a template (PDB 6a5d.1A).
731

732 # RESOURCE AVAILABILITY

733

734 ## Lead Contact

735 Further information and requests for resources and reagents should be directed to and
736 will be fulfilled by the Lead Contact, Ueli Grossniklaus (grossnik@botinst.uzh.ch).
737

738 ## Materials Availability,

739 Requests for other strains and plasmids should be directed to the Lead Contact.
740

Data and Code Availability.

This study did not generate datasets or code.

EXPERIMENTAL MODEL AND SUBJECT DETAILS

M. polymorpha subsp. ruderalis plants were grown on sterile culture on half-strength Gamborg's B5 basal medium (PhytoTechnology Laboratories), supplemented with 1% phytoagar in Petri dishes sealed with air-permeable tape. The plants were kept under fluorescent light and long-day conditions (16 h light at 22ºC, 8 h dark at 20 ºC) in Percival growth cabinets (models AR-41L3 and AR-41/L2). Alternatively, to induce sexual reproduction, plants were cultivated in jiffy pots filled with a 1:1 mixture of soil ("Einheitserde D73 + Bims", Universalerde) and sand or in culture boxes in sterile culture on half-strength Gamborg's B5 basal medium (Duchefa Eco2 Box, #E1654), under fluorescent light supplemented with far-red light (GreenPower LED module HF far-red, #929000464503 and #929000632103 Philips).

Wild-type (WT) plants in all experiments were Arabidopsis thaliana L. (Heyn) accession Ler-0. The At*fer-2* mutant was obtained from the Signal Collection at the Salk Institute. Plants were grown in soil (ED73; Universalerde), covered with a thin quartz sand layer, under long photoperiods (16 hs light/8 hs dark) at 23°C and 60% relative humidity.

METHOD DETAILS

Phylogenetic analysis

Protein sequences were identified in plant genomes via BLASTp searches in https://phytozome.jgi.doe.gov/pz/portal.html. To elucidate the evolutionary relationship across land plant evolutionary history, we focused on *A. thaliana, Selaginella*

765 *moellendorffii, Physcomitrella patens* and *M. polymorpha*, as representative species for
766 angiosperms, lycophytes, mosses and liverworts, respectively. Complete or partial coding
767 protein sequences were aligned using the ClustalW parameters and were conducted in
768 MEGA7. Phylogenetic trees were constructed with Neighbor-joining method, with a
769 bootstrap test of 1000 replicates. The evolutionary distances were computed using the
770 Poisson correction method.
771
772 **Vector construction**
773 Expression constructs: a BJ36 plasmid [77] containing a tripleVENUS-NLS (trpVNS)
774 fragment was modified by adding a ligation-independent cloning (LiC) adapter site [78].
775 A promoter fragment of Mp*FER* of 3.2 kb was amplified using primers specified below
776 and cloned into the BJ36 vector via LiC cloning. $_{pro}$Mp*FER* promoter fragment fused to
777 trpVNS was then shuttled via *Not*I restriction sites into the HART01 [77] expression
778 vector. The expression vector was also directly modified to contain the LiC sites, so
779 promoter fragments can now be directly cloned in front of the trpVNS in the HART01
780 vector via LiC-cloning. This vector was called VHL (trpVNS-containing HART01 vector
781 with LiC sites).
782 amiRNA constructs: For functional analyses three independent artificial microRNA
783 (amiRNA) constructs were made (Figure S2). The endogenous microRNA precursor
784 Mp*miR160* was used as both backbone and template to design the constructs which
785 generate single species small RNA molecules of 21 nt length, complementary to the
786 target gene transcript [63,79]. Three miR160 backbones containing independent amiR-
787 Mp*FER*/amiR-Mp*FER** duplexes were synthesized by GenScript and fused to the
788 $_{pro}$Mp*EF1* promoter in the BJ36 shuttle vector and shuttled to the HART01 expression
789 vector as described previously [79]. The folding structure and design procedures were

790 explained in detail in [63,79]. The sequences for the amiRNAs were designed to retain
791 the exact physical properties of the endogenous Mp*miR160* template. The folding
792 patterns were analyzed in the Mfold software [80] and the sequences synthesized (Figure
793 S2).
794 CRISPR/Cas gRNA: Selection of target sites was done using CasFinder [81].
795 Complementary oligos were designed and annealed for ligation into gRNA, in the
796 pMpGE_En03 vector, previously digested with BsaI restriction enzyme. Resulting gRNAs
797 were incorporated into binary vector pMpGE011 through gateway recombination.
798 Over-expression of Mp*FER* and At*FER*: The full-length Mp*FER* sequence was amplified
799 from genomic *M. polymorpha* DNA with attB sites and Gateway-cloned via pDONR207.
800 For *A. thaliana* expression, Mp*FER* was introduced into the expression vectors
801 pMDC201, which contains a *2X35S* promoter fragment and an in-frame C-terminal
802 mGFP6 [82]. For *M. polymorpha* expression, Mp*FER* was introduced intro the binary
803 vector pMpGWB308, which contains a MpEF1 promoter and an in-frame C-terminal
804 citrine [83]. Similarly, for expression of At*FER* in *M. polymorpha*, coding sequence of
805 AtFER was introduced into pMpGWB308 binary vector, for the generation of
806 $_{pro}$Mp*EF1:*At*FER-Cit* construct.
807

808 **Quantitative real-time PCR (qRT-PCR) and droplet digital PCR (ddPCR)**

809 RNA extraction from *M. polymorpha*: RNA extraction from thallus tissue (ca. 100mg
810 including apical notch) was done using the Rneasy plant mini kit (#74904, Qiagen). To
811 remove contaminating DNA, the TURBO DNAfree™ Kit (AM1907 Ambion) was used
812 according to manufacturer's recommendations. To extract RNA from the gametophores
813 (2 antheridiophores > 5mm diameter were pooled, respectively, for each replicate), the
814 Direct(-zol) RNA MiniPrep (#R2050, ZymoResearch) was used with TRIzol Reagent

(#15596026, Ambion) according to the manufacturer's protocol, including on-column DNase digestion and subsequent TURBO DNA-free™ Kit (AM1907 Ambion) treatment. RNA samples were quantified using the Qubit® RNA HS Assay Kit (#Q32852, Life Technologies), a Nanodrop ND-1000 Spectrometer or an Agilent 2100 BioAnalyzer.

cDNA synthesis: cDNA was synthesized from 0.5 µg or 1.0 µg of total RNA. Reverse transcription was performed in 25 µl with 20µg/ml Oligo(dT) 12-18 primers and 200 units of SuperScript® II Reverse Transcriptase (#18064-014, Invitrogen) according to the manufacturer's protocol. The resulting cDNA was diluted 1:9 by adding nuclease-free water. To control for genomic DNA contamination, control replicates of all samples were incubated without SuperScript® II reverse transcriptase.

Primer tests and quantitative RT-PCR: Primer efficiency and concentration tests were carried out for Mp*FER* and suitable reference genes as described previously (Rövekamp et al., 2016, Althoff et al., 2014). Amplification experiments were carried out using a 7500 Applied Biosystem Fast Real-Time PCR System. Reactions were performed in 20 µl volumes containing 10 µl 2X SYBR-green mastermix (SsoAdvanced™ Universal SYBRGreen Supermix), 200 nM (Mp*EF1* and Mp*FER*) or 250 nM (Mp*ACTIN*) forward and reverse primers, and 1 µl diluted cDNA. Where possible, three technical and biological replicates were performed for each reaction. The primers used for the qRT-PCR are summarized in Table S1.

For ddPCR analysis, individual PCR reactions were performed in a total volume of 25 µl, using 1X ddPCR EvaGreen Supermix, with droplets generated according to manufacturer's recommendations. Reading of the PCR-amplified droplets was carried out by the QX200 Droplet Reader (Bio-Rad) and analysed by the QuantaSoft TM Software (v1.4, Bio-Rad). The counts from ddPCR were normalised through a log2 transformation. Afterwards, relative expression was calculated against the geometric mean of the counts

for all three reference genes (Mp*ACT1*, Mp*ACT7*, and Mp*APT3*) [84]: (log2(gene tested + 1) - log2(geom. mean of all references + 1)). The primers used for the ddPCR are summarized in Table S1.

Transformation into *M. polymorpha* and *A. thaliana*

Agrobacterium-mediated transformation using regenerating thalli of *M. polymorpha* was done by co-cultivation 15-days old Marchantia fragments with transformed *Agrobacterium tumefaciens* (GV3101) cells [85,86]. After three days of incubation, positive transformants were selected on Gamborg's B5 plates supplemented with 10 *μ*g/ml Hygromicin B (Invitrogen), 0.5 μM Chlorosulfuron or Kanamycin, and 100 μg/ml of Cefotaxime sodium. Isogenic lines were obtained by using plants derived from gemmae of the T1 generation (G1 generation). G1 or subsequent gemmae generations were used for all experiments, as they are derived from single cells [87,88]. Transformation of *A. thaliana* via *A. tumefaciens* (GV3101) was performed by floral dipping according to [89]. Primers used for amplification of promoter fragments of Mp*FER* are listed in Table S2.

Microscopy

Plants were observed in a Lumar.V12 (Zeiss) or a Leica MZFLIII dissection microscope and photographed with an AxioCam HRc (Zeiss) or Leica DFC 420C camera. Clearings were observed using a Leica DMR microscope and photographed with an Axiocam 105 color camera. Fluorescence reporter expression were analyzed using a Leica SP5 confocal microscope. Fiji [90] and GIMP (version 2.8.10) software were used for adjustments of brightness, contrast, channel selection, and image size.

Tissue clearing for bright field microscopy: *M. polymorpha* tissues were fixed in Carnoy's solution and incubated at 4^{o}C overnight, followed by rehydration in an ethanol series of

85%, 70%, 50%, and 30%. Samples were incubated for 1 hour at 4°C for each step and then incubated in chloral hydrate solution at 4°C overnight. Samples were mounted in chloral hydrate.

Calcofluor-white staining for cell size measurements: Pieces of fresh thallus tissue located in fully differentiated zones [91] of plants grown on plates were dissected out and put into water. The pieces were transferred to PBS pH 6.1 containing 100 *µ*g/ml Calcofluor-white and vacuum-infiltrated for 1 hour before being mounted on slides. The area of the epidermal cells was measured using Imaris 8.3.1. software. Cells of air pores and the two adjacent cell layers were excluded from the analysis, as well as the spiralling cells surrounding newly developing air pores.

For cell-death staining, seven-days old gemmalings were stained with lactophenol-trypanblue (10 mL of lactic acid, 10 mL of glycerol, 10 g of phenol, 10 mg of trypan blue, dissolved in 10 mL of distilled water) and boiled for approximately 1 min in the stain solution and then decolorized in chloral hydrate (2.5 g of chloral hydrate dissolved in 1 mL of distilled water) for at least 30 min. They were mounted in chloral hydrate and imaged in dissecting microscope.

Western blot analysis

M. polymorpha explants were ground in liquid nitrogen and resuspended in 300 µL of Laemmli buffer [92]. After centrifugation at 6,000 rpm for 5 min at 4˚C, the supernatant was recovered. Protein accumulation was confirmed by Western blotting, using the anti-GFP antibody (1:3000, Torrey Pines Biolabs). As secondary antibodies, the Agrisera S09602 goat anti-rabbit antibody was used with the ECL-chemistry of FUSION FX - Western Blot & Chemi Imaging (Vilber Lourmat).

Growth rate experiments

Gemmae of wild-type, Mp*fer-1*, and independent transformation lines of amiR-Mp*FER* lines were grown on plates and the thallus area was measured over time. 10 or 30 gemmae of four independent transformation lines were grown on half-strength Gamborg's B5 and scanned on an Epson 2450 Photo scanner at 600dpi. Plant area was measured using color threshold settings and particle analysis in the Fiji software [90].

Expression map

Gene expression of *Cr*RLK1L signaling pathway components was calculated from publicly available RNA-seq data of 39 samples of *M. polymorpha* Tak-1 and Tak.2. Samples were grouped by tissue and analyzed under the same pipeline: Nextera paired-end adapters were trimmed from sequencing reads using the bbduk tool embedded in the BBMap software package [93]. Read ends with quality below 20 were also trimmed and the minimum read length was set to 25. The rest of parameters of bbduk were set as default. Reads were mapped to *M. polymorpha* reference genome (v3.1) [45] using the Tophat software (v2.1.1) [94], designed for RNA-sequencing read mapping. Tophat contains Bowtie (v2.3.2.0) [95] as the aligner software. All parameters were set to default values except for the RAM memory and number of used Cores. Mapped reads were sorted using samtools (v1.3.1) [96] and counted with the software HTSeq-count" (v.0.9.1) [97]. Gene expression values were calculated using the package DESeq2 (Release 3.6) [98] for R software (v3.4.4) [99]. Another R package, ggplot2 (release 2.2.1) [100] was used for producing the figures. A summary of the samples that were used in this study is provided in Table S3.

Three-dimensional (3D) protein structure modeling

Comparative modeling of protein 3D structures was performed using the SWISS-MODEL online-tool [60]. The software was fed with the three protein sequences of MpFER, MpRALF1, and MpLRE1 as input to model, and one PDB file as a 3D template, which contains the published crystal structure of the protein complex formed by AtFER, AtRALF23, and AtLLG2 [35]. Quality control of the model was assessed using the same tool and the results are summarized in Figure S5E. Spatial comparisons of the *M. polymorpha* predicted structures with the crystal structures of *A. thaliana* were performed in PyMol [101].

QUANTIFICATION AND STATISTICAL ANALYSIS

Analyses were performed in InfoStat (http://www.infostat.com.ar). Tests are indicated in the corresponding figure legend.

References

1. Showalter AM. (1993). Structure and function of plant cell wall proteins. Plant Cell *5*, 9–23.

2. Franck CM, Westermann J, Boisson-Dernier A. (2018). Plant malectin-like receptor kinases: from cell wall integrity to immunity and beyond. Annu Rev Plant Biol *69*, 301–328.

3. Shiu SH, Bleecker AB. (2001). Plant receptor-like kinase gene family: diversity, function, and signaling. Sci STKE *2001*, re22.

4. Steinwand BJ, Kieber JJ. (2010). The role of receptor-like kinases in regulating cell wall function. Plant Physiol. *153*, 479–84.

5. Wolf S, Hématy K, Hofte H. (2012). Growth control and cell wall signaling in plants. Annu Rev Plant Biol *63*, 381–407.

6. Escobar-Restrepo J-M, Huck N, Kessler S, Gagliardini V, Gheyselinck J, et al. (2007). The FERONIA receptor-like kinase mediates male-female interactions during pollen tube reception. Science *317*, 656–660.

7. Hématy K, Sado PE, Van Tuinen A, Rochange S, Desnos T, et al. (2007). A receptor-like kinase mediates the response of *Arabidopsis* cells to the inhibition of cellulose synthesis. Curr Biol. *17*, 922–931.

8. Boisson-Dernier A, Roy S, Kritsas K, Grobei MA, Jaciubek M, Schroeder, J.I., Grossniklaus, U. (2009). Disruption of the pollen-expressed *FERONIA* homologs *ANXUR1* and *ANXUR2* triggers pollen tube discharge. Development *136*, 3279–3288.

9. Guo H, Li L, Ye H, Yu X, Algreen A, Yin Y. (2009). Three related receptor-like kinases are required for optimal cell elongation in *Arabidopsis thaliana*. Proc Natl Acad Sci USA *106*, 7648–7653.

10. Guo H, Ye H, Li L, Yin Y. (2009). A family of receptor-like kinases are regulated by *BES1* and involved in plant growth in *Arabidopsis thaliana*. Plant Signal Behav *4*, 784–786.

11. Kessler SA, Shimosato-Asano H, Keinath NF, Wuest SE, Ingram G, et al. (2010). Conserved molecular components for pollen tube reception and fungal invasion. Science *330*, 968–971.

12. Bai L, Ma X, Zhang G, Song S, Zhou Y, et al. (2014). A receptor-like kinase mediates ammonium homeostasis and is important for the polar growth of root hairs in *Arabidopsis*. Plant Cell *26*, 1497–511.

13. Schoenaers S, Balcerowicz D, Breen G, Hill K, Zdanio M, Mouille G, Holman TJ, Oh J, Wilson MH, et al., (2018). The auxin-regulated *Cr*RLK1L kinase ERULUS controls cell wall composition during root hair tip growth. Curr. Biol. *28*, 722–732.

14. Miyazaki S, Murata T, Sakurai-Ozato N, Kubo M, Demura T, et al. (2009). *ANXUR1* and *2*, sister genes to *FERONIA*/*SIRENE*, are male factors for coordinated fertilization. Curr Biol. *19*, 1327–1331.

15. Keinath NF, Kierszniowska S, Lorek J, Bourdais G, Kessler SA, Shimosato-Asano H, Grossniklaus U, Schulze WX, Robatzek S, Panstruga RJ (2010). PAMP (pathogen-associated molecular pattern)-induced changes in plasma membrane compartmentalization reveal novel components of plant immunity. J Biol Chem *285*, 39140–39149.

16. Duan Q, Kita D, Li C, Cheung AY, Wu HM. (2010). FERONIA receptor-like kinase regulates RHO GTPase signaling of root hair development. Proc Natl Acad Sci USA *107*, 17821–17826.

17. Galindo-Trigo S, Blanco-Touriñán N, DeFalco TA, Wells ES, Gray JE, Zipfel C, Smith LM. (2020). *Cr*RLK1L receptor-like kinases HERK1 and ANJEA are female determinants of pollen tube reception. EMBO Rep *21*, e48466.

18. Zhu L, Chu LC, Liang Y, Zhang XQ, Chen LQ, Ye D. (2018). The *Arabidopsis Cr*RLK1L protein kinases BUPS1 and BUPS2 are required for normal growth of pollen tubes in the pistil. Plant J *95*, 474–486.

19. Li C, Yeh F-L,Cheung AY, Duan Q, KitaD, et al. (2015). Glycosylphosphatidylinositol-anchored proteins as chaperones and co-receptors for FERONIA receptor kinase signaling in *Arabidopsis*. eLife *4*, e06587.

20. Richter J, Ploderer M, Mongelard G, Gutierrez L, Hauser MT. (2017). Role of *Cr*RLK1L cell wall sensors HERCULES1 and 2, THESEUS1, and FERONIA in growth adaptation triggered by heavy metals and trace elements. Front Plant Sci *8*, 1554.

21. Richter J, Watson JM, Stasnik P, Borowska M, Neuhold J, Berger M, Stolt-Bergner P, Schoft V, Hauser MT. (2018). Multiplex mutagenesis of four clustered *Cr*RLK1L with CRISPR/Cas9 exposes their growth regulatory roles in response to metal ions. Sci Rep *8*, 12182.

22. Stegmann M, Monaghan J, Smakowska-Luzan E, Rovenich H, Lehner A, et al. (2017). The receptor kinase FER is a RALF-regulated scaffold controlling plant immune signaling. Science *355*, 287–289.

23. Ngo QA, Vogler H, Lituiev DS, Nestorova A, Grossniklaus U. (2014). A calcium dialog mediated by the *FERONIA* signal transduction pathway controls plant sperm delivery. Dev Cell *29*, 491–500.

24. Yu F, Qian L, Nibau C, Duan Q, Kita D, et al. (2012). *FERONIA* receptor kinase pathway suppresses abscisic acid signaling in *Arabidopsis* by activating ABI2 phosphatase. Proc Natl Acad Sci USA *109*, 14693–14698.

25. Mao D, Yu F, Li J, Van de Poel B, Tan D, et al. (2015). FERONIA receptor kinase interacts with S-adenosylmethionine synthetase and suppresses S-adenosylmethionine production and ethylene biosynthesis in *Arabidopsis*. Plant Cell Env. *38*, 2566–2574.

26. Deslauriers SD, Larsen PB. (2010). *FERONIA* is a keymodulator of brassinosteroid and ethylene responsiveness in *Arabidopsis* hypocotyls. Mol Plant *3*, 626–640.

27. Shih H-W, Miller ND, Dai C, Spalding EP, Monshausen GB. (2014). The receptor-like kinase FERONIA is required for mechanical signal transduction in *Arabidopsis* seedlings. Curr Biol. *24*, 1887–1892.

28. Denness L, McKenna JF, Segonzac C, Wormit A, Madhou P, et al. (2011). Cell wall damage-induced lignin biosynthesis is regulated by a reactive oxygen species- and jasmonic acid-dependent process in *Arabidopsis*. Plant Physiol *156*, 1367–1374.

29. Okuda S, Tsutsui H, Shiina K, Sprunck S, Takeuchi H, Yui R, Kasahara RD, Hamamura Y, Mizukami A, Susaki D, Kawano N, Sakakibara T, Namiki S, Itoh K, Otsuka K, Matsuzaki M, Nozaki H, Kuroiwa T, Nakano A, Kanaoka MM, Dresselhaus T, Sasaki N, Higashiyama T. (2009). Defensin-like polypeptide LUREs are pollen tube attractants secreted from synergid cells. Nature *458*, 357–361.

30. Huck N, Moore JM, Federer M, Grossniklaus U. (2003). The *Arabidopsis* mutant *feronia* disrupts the female gametophytic control of pollen tube reception. Development *130*, 2149–2159.

31. Rotman N, Rozier F, Boavida L, Dumas C, Berger F, Faure J-E. (2003). Female control of male gamete delivery during fertilization in *Arabidopsis thaliana*. Curr Biol. *13*, 432–436.

32. Ge Z, Bergonci T, Zhao Y, Zou Y, Du S, et al. (2017). *Arabidopsis* pollen tube integrity and sperm release are regulated by RALF-mediated signaling. Science *358*, 1596–1600.

33. Haruta M, Sabat G, Stecker K, Minkoff BB, Sussman MR. (2014). A peptide hormone and its receptor protein kinase regulate plant cell expansion. Science *343*, 408–411.

34. Dünser K, Gupta S, Herger A, Feraru MI, Ringli C, Kleine-Vehn J. (2019). Extracellular matrix sensing by FERONIA and Leucine-Rich Repeat Extensins controls vacuolar expansion during cellular elongation in *Arabidopsis thaliana*. EMBO J *38*, pii: e100353.

35. Xiao Y, Stegmann M, Han Z, DeFalco TA, Parys K, Xu L, Belkhadir Y, Zipfel C, Chai J. (2019). Mechanisms of RALF peptide perception by a heterotypic receptor complex. Nature *572*, 270–274.

36. Mecchia MA, Santos-Fernandez G, Duss NN, Somoza SC, Boisson-Dernier A, et al. (2017). RALF4/19 peptides interact with LRX proteins to control pollen tube growth in *Arabidopsis*. Science *358*, 1600–1603.

37. Capron A, Gourgues M, Neiva LS, Faure J-E, Berger F, Pagnussat G, Krishnan A, Alvarez-Mejia C, Vielle-Calzada JP, Lee YR, Liu B, Sundaresan V. (2008). Maternal control of male-gamete delivery in *Arabidopsis* involves a putative GPI-anchored protein encoded by the *LORELEI* gene. Plant Cell *20*, 3038–3049.

38. Boisson-Dernier A, Kessler SA, Grossniklaus U. (2011). The walls have ears: the role of plant *Cr*RLK1Ls in sensing and transducing extracellular signals. J Exp Bot *62*.

39. Hématy K, Höfte H. (2008). Novel receptor kinases involved in growth regulation. Curr Opin Plant Biol. *11*, 321–328.

40. Cheung AY, Wu HM. (2011). THESEUS 1, FERONIA and relatives: a family of cell wall-sensing receptor kinases? Curr Opin Plant Biol *14*, 632–641.

41. Nissen KS, Willats WGT, Malinovsky FG. (2016). Understanding *Cr*RLK1L function: cell walls and growth control. Trends Plant Sci *21*, 516–527.

42. Feng W, Kita D, Peaucelle A, Cartwright HN, Doan V, Duan Q, Liu MC, Maman J, Steinhorst L, Schmitz-Thom I, Yvon R, Kudla J, Wu HM, Cheung AY, Dinneny JR. (2018). The FERONIA receptor kinase maintains cell-wall integrity during salt stress through Ca^{2+} signaling. Curr Biol. *28*, 666–675.

43. Lindner H, Müller LM, Boisson-Dernier A, Grossniklaus U. (2012). *Cr*RLK1L receptor-like kinases: not just another brick in the wall. Curr Opin Plant Biol *15*, 656–669.

44. Galindo-Trigo S, Gray JE, Smith LM. (2016). Conserved roles of *Cr*RLK1L receptor-like kinases in cell expansion and reproduction from algae to angiosperms. Front Plant Sci *7*, 1269.

45. Bowman JL, Kohchi T, Yamato KT, Jenkins J, Shu S, Ishizaki K, et al. (2017). Insights into land plant evolution garnered from the *Marchantia polymorpha* genome. Cell *171*, 287-304.e15.

46. Rövekamp M, Bowman JL, Grossniklaus U. (2014). Back to the rhizoids of plant sexual development. Abstr. 23rd Intl. Congr. Sex. Plant Reprod. Porto Port., https://www.fc.up.pt/sprporto2014/doc/23rd%20International%20congress%20on%20sexual%20plant%20reproduction%20ABSBook.pdf.

47. Bowman JL, Floyd SK, Sakakibara K (2007). Green genes-comparative genomics of the green branch of life. Cell *129*, 229–234.

48. Nishiyama T, Fujita T, Shin-I T, Seki M, Nishide H, Uchiyama I, Kamiya A, Carninci P, Hayashizaki Y, Shinozaki K, et al. (2003). Comparative genomics of *Physcomitrella patens* gametophytic transcriptome and *Arabidopsis thaliana*: implication for land plant evolution. Proc Natl Acad Sci USA *100*, 8007–8012.

49. Qiu YL, Li L, Wang B, Chen Z, Knoop V, Groth-Malonek M, Dombrovska O, Lee J, Kent L, Rest J, et al. (2006). The deepest divergences in land plants inferred from phylogenomic evidence. Proc Natl Acad Sci USA *103*, 15511–15516.

50. Wickett NJ, Mirarab S, Nguyen N, Warnow T, Carpenter E, Matasci N, Ayyampalayam S, Barker MS, Burleigh JG, Gitzendanner MA, et al. (2014). Phylotranscriptomic analysis of the origin and early diversification of land plants. Proc Natl Acad Sci USA *1111*, E4859–E4868.

51. Mishler BD, Churchill SP (1984). A cladistic approach to the phylogeny of the "bryophytes." Brittonia *36*, 406–424.

52. Kenrick P, Crane PR (1997). The origin and early evolution of plants on land. Nature *389*, 33–39.

53. Floyd SK, Bowman JL. (2007). The ancestral developmental tool kit of land plants. Int J Plant Sci *168*, 1–35.

54. Bowman JL, Araki T, Arteaga-Vazquez MA, Berger F, Dolan L, Haseloff J, Ishizaki K, Kyozuka J, Lin SS, Nagasaki H, Nakagami H, Nakajima K, Nakamura Y, Ohashi-Ito K, Sawa S, Shimamura M, Solano R, Tsukaya H, Ueda T, Watanabe Y, Yamato KT, Zachgo S, Kohchi T (2016). The naming of names: guidelines for gene nomenclature in *Marchantia*. Plant Cell Physiol *57*, 257–261.

55. Ishizaki K (2017). Evolution of land plants: insights from molecular studies on basal lineages. Biosci Biotechnol Biochem *81*, 73–80.

56. Honkanen S, Jones VAS, Morieri G, Champion C, Hetherington AJ, Kelly S, Proust H, Saint-Marcoux D, Prescott H, Dolan L. (2016). The mechanism forming the cell surface of tip-growing rooting cells Is conserved among land plants. Curr Biol. *26*, 3238–3244.

57. Westermann J, Streubel S, Franck CM, Lentz R, Dolan L, Boisson-Dernier A. (2019). An evolutionarily conserved receptor-like kinases signaling module controls cell wall integrity during tip growth. Curr Biol. *29*, 4153.

58. Kessler SA, Lindner H, Jones DS, Grossniklaus U. (2014). Functional analysis of related *Cr*RLK1L receptor-like kinases in pollen tube reception. EMBO Rep *16*, 107–115.

59. Hirano N, Marukawa Y, Abe J, Hashiba S, Ichikawa M, Tanabe Y, (2015). A receptor-like kinase, related to cell wall sensor of higher plants, is required for sexual reproduction in the unicellular Charophycean alga, *Closterium peracerosum–strigosum– littorale* Complex. Plant Cell Physiol *56*, 1456–1462.

60. Schwede T, Kopp J, Guex N, Peitsch MC (2003). SWISS-MODEL: an automated protein homology-modeling server. Nucleic Acids Res. *31*, 3381–3385.

61. Liu L, Zheng C, Kuang B, Wei L, Yan L, Wang T (2016). Receptor-like kinase RUPO interacts with potassium transporters to regulate pollen tube growth and integrity in rice. PLoS Genet *12*, e1006085.

62. Schulze-Muth P, Irmler S, Schröder G, Schröder J (1996). Novel type of receptor-like protein kinase from a higher plant (*Catharanthus roseus*): cDNA, gene, intramolecular autophosphorylation, and identification of a threonine important for auto- and substrate phosphorylation. J Biol Chem *271*, 26684–26689.

63. Flores-Sandoval E, Dierschke T, Fisher TJ, Bowman JL (2016). Efficient and inducible use of artificial microRNAs in *Marchantia polymorpha*. Plant Cell Physiol *57*, 281–290.

64. Althoff F, Kopischke S, Zobell O, Ide K, Ishizaki K, Kohchi T, Zachgo S. (2014). Comparison of the Mp*EF1α* and CaMV35 promoters for application in *Marchantia polymorpha* overexpression studies. Transgenic Res. *23*, 235–244.

65. Gonneau M, Desprez T, Martin M, Doblas VG, Bacete L, Miart F, Sormani R, Hématy K, Renou J, Landrein B et al. (2018). Receptor kinase THESEUS1 is a RAPID ALKALINIZATION FACTOR34 receptor in *Arabidopsis*. Curr Biol. *28*, 2452–2458.

66. Gachomo EW, Jno Baptiste L, Kefela T, Saidel WM, Kotchoni SO (2014). The *Arabidopsis CURVY1* (*CVY1*) gene encoding a novel receptor-like protein kinase regulates cell morphogenesis, flowering time and seed production. BMC Plant Biol *14*, 221.

67. Merz D, Richter J, Gonneau M, Sanchez-Rodriguez C, Eder T, Sormani R, Martin M, Hématy K, Höfte H, Hauser MT (2017). T-DNA alleles of the receptor kinase THESEUS1 with opposing effects on cell wall integrity signaling. J Exp Bot *68*, 4583–4593.

68. Chiyoda S, Ishizaki K, Kataoka H, Yamato KT, Kohchi T (2008). Direct transformation of the liverwort *Marchantia polymorpha* L. by particle bombardment using immature thalli developing from spores. Plant Cell Rep *27*, 1467–1473.

69. Srivastava R, Liu JX, Guo H, Yin Y, Howell SH (2009). Regulation and processing of a plant peptide hormone, AtRALF23, in *Arabidopsis*. Plant J *59*, 930–939.

70. Boisson-Dernier A, Franck CM, Lituiev DS, Grossniklaus U. (2015). Receptor-like cytoplasmic kinase MARIS functions downstream of *Cr*RLK1L-dependent signaling during tip growth. Proc Natl Acad Sci USA *112*, 12211–12216.

71. Liao H-Z, Zhu M-M, Cui H-H, Du X-Y, Tang Y, et al. (2016). *MARIS* plays important roles in *Arabidopsis* pollen tube and root hair growth. J Integr Plant Biol *58*, 927–940.

72. Bowen EJ (1935). A note on the conduction of water in *Fimbriaria bleumeana*. Ann. Bot. *49*, 844–848.

73. Fujikura U, Elsaesser L, Breuninger H, Sánchez-Rodríguez C, Ivakov A, Laux T, Findlay K, Persson S, Lenhard M. (2014). Atkinesin-13A modulates cell-wall synthesis and cell expansion in *Arabidopsis thaliana* via the *THESEUS1* pathway. PLoS Genet *10*, e1004627.

74. Pierik R, Tholen D, Poorter H, Visser EJ, Voesenek LA (2006). The Janus face of ethylene: growth inhibition and stimulation. Trends Plant Sci *11*, 176–183.

75. Wolf S, Höfte H. (2014). Growth control: a saga of cell walls, ROS, and peptide receptors. Plant Cell *26*, 1848–1856.

76. Humplík JF, Bergougnoux V, Van Volkenburgh E (2017). To stimulate or inhibit? That Is the question for the function of abscisic acid. Trends Plant Sci *22*, 830–841.

77. Flores-Sandoval E, Eklund DM, Bowman, JL (2015). A simple auxin transcriptional response system regulates multiple morphogenetic processes in the liverwort *Marchantia polymorpha*. PLoS Genet *11*, e1005207.

78. De Rybel B, van den Berg W, Lokerse AS., Liao C-Y, van Mourik H, Moller B, Llavata-Peris CI, Weijers D (2011). A versatile set of ligation-independent cloning vectors for functional studies in plants. Plant Physiol. *156*, 1292–1299.

79. Rövekamp M, Bowman JL, Grossniklaus U (2016). *Marchantia* Mp*RKD* regulates the gametophyte-sporophyte transition by keeping egg cells quiescent in the absence of fertilization. Curr. Biol. *26*, 1782–1789.

80. Zuker M. (2003). Mfold web server for nucleic acid folding and hybridization prediction. Nucleic Acids Res *31*, 3406–3415.

81. Aach J, Mali P, Church GM (2014). CasFinder: flexible algorithm for identifying specific Cas9 targets in genomes. BioRxiv Doi 101101005074.

82. Curtis MD, Grossniklaus U (2003). A Gateway cloning vector set for high-throughput functional analysis of genes *in planta*. Plant Physiol. *133*, 462–469.

83. Ishizaki K, Nishihama R, Ueda M, Inoue K, Ishida S, Nishimura Y, Shikanai T, Kohchi T (2015). Development of Gateway binary vector series with four different selection markers for the liverwort *Marchantia polymorpha*. PLoS ONE *10*, e0138876.

84. Vandesompele J, De Preter K, Pattyn F, Poppe B, Van Roy N, De Paepe A, Speleman F. (2002). Accurate normalization of real-time quantitative RT-PCR data by geometric averaging of multiple internal control genes. Genome Biol *3*, RESEARCH0034.

85. Kubota A, Ishizaki K, Hosaka M, Kohchi T (2013). Efficient *Agrobacterium*-mediated transformation of the liverwort *Marchantia polymorpha* using regenerating thalli. Biosci Biotechnol Biochem *77*, 167–172.

86. Ishizaki K, Chiyoda S, Yamato KT, Kohchi, T (2008). *Agrobacterium*-mediated transformation of the haploid liverwort *Marchantia polymorpha* L., an emerging model for plant biology. Plant Cell Physiol. *49*, 1084–1091.

87. Barnes CR, Land WJG. (1907). Bryological papers. I. The origin of air chambers. Bot Gaz *44*, 197–213.

88. Hughes SJ (1971). On conidia of fungi, and gemmae of algae, bryophytes, and pteridophytes. Can J Bot *49*, 1319–1339.

89. Bent A. (2006). *Agrobacterium* protocols. Totowa NJ Humana Press *Volume I*.

90. Schindelin J, Arganda-Carreras I, Frise E, Kaynig V, Longair M, Pietzsch T, Preibisch S, et al. (2012). Fiji: An open-source platform for biological-image analysis. Nat. Methods *9*, 676–682.

91. Solly JE, Cunniffe NJ Harrison CJ (2017). Regional growth rate differences specified by apical notch activities regulate liverwort thallus shape. Curr. Biol. *27*, 16–26.

92. Laemmli UK (1970). Cleavage of structural proteins during the assembly of the head of bacteriophage T4. Nature *227*, 680–685.

93. Bushnell B (2014). BBMap: a fast, accurate, splice-aware aligner (No. LBNL-7065E). Lawrence Berkeley Natl. LabLBNL Berkeley, CA, USA.

94. Trapnell C, Pachter L, Salzberg SL (2009). TopHat: discovering splice junctions with RNA-Seq. Bioinformatics *25*, 1105–1111.

95. Langdon WB (2015). Performance of genetic programming optimised Bowtie2 on genome comparison and analytic testing (GCAT) benchmarks. BioData Min. *8*, 1.

96. Li H, Handsaker B, Wysoker A, Fennell T, Ruan J, Homer N, et al (2009). The sequence alignment/map format and SAMtools. Bioinformatics *25*, 2078–2079.

97. Anders S, Pyl PT, Huber W. (2015). HTSeq—a Python framework to work with high-throughput sequencing data. Bioinformatics *31*, 166–169.

98. Love MI, Huber W, Anders S (2014). Moderated estimation of fold change and dispersion for RNA-seq data with DESeq2. Genome Biol. *15*, 550.

99. Team RC (2013). R: A language and environment for statistical computing.

100. Wickham H (2016). ggplot2: elegant graphics for data analysis. *Springer*.

101. DeLano WL (2002). Pymol: An open-source molecular graphics tool. CCP4 Newsl. Protein Crystallogr. *40*, 82–92.

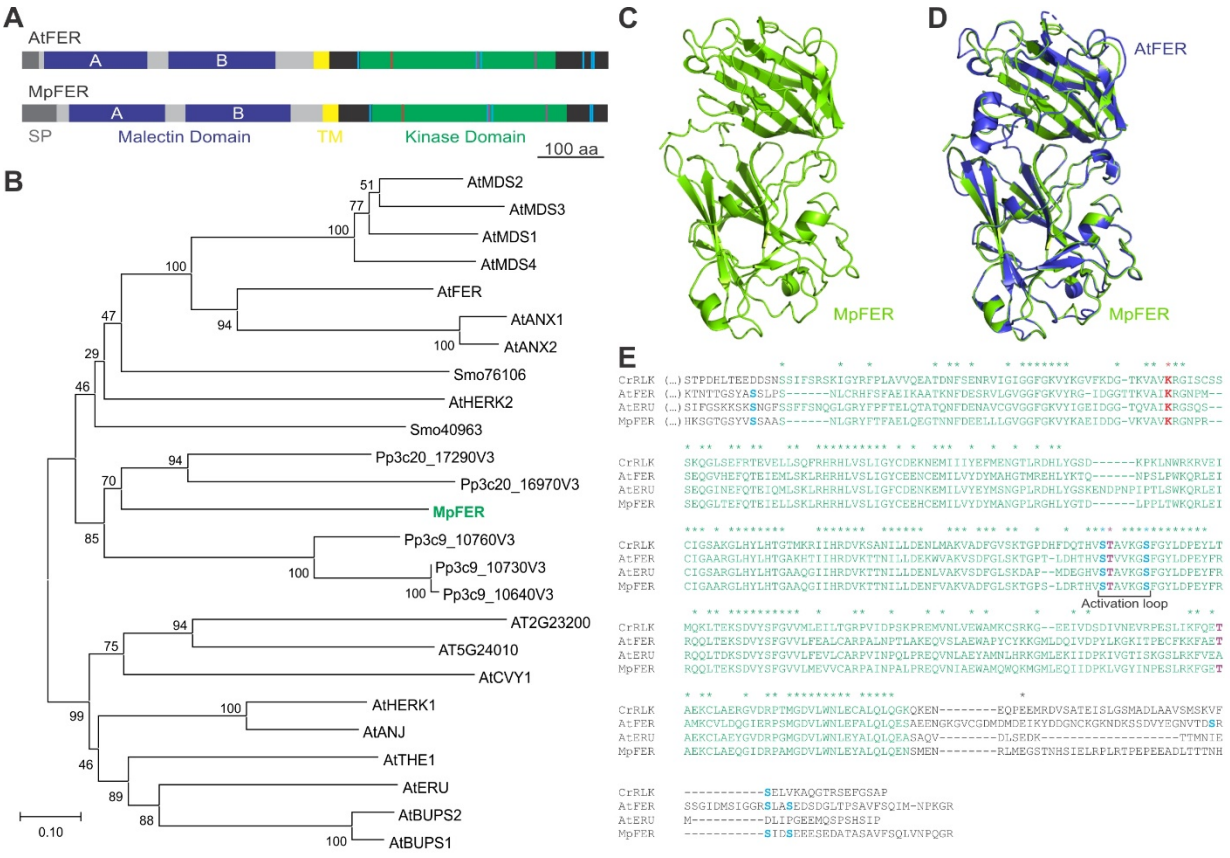

Figure 1. *Cr*RLK1Ls Are Conserved among Land Plants

(A) Representation of AtFER and MpFER proteins. Malectin-like domains are represented in blue and kinase domains in green. SP, signal peptide; TM, transmembrane domain (yellow). Amino acids important for regulation and activity are marked in red, violet, and light blue as described in Figure 1E.

(B) A rooted neighbor-joining tree of the amino acid sequence of the predicted malectin-like domain. *Cr*RLK1L members from *Marchantia polymorpha* (Mp), *Physcomitrella patens* (Pp), *Selaginella moellendorffii* (Smo), and *Arabidopsis thaliana* (At) were used. The numbers indicate the bootstrap values (%) from 1000 replications. The given scale represents a substitution frequency of 0.1 amino acids per site.

(C) Cartoon representation of the predicted three-dimensional structure of the MpFER malectin-like domain, showing predicted alpha-helix and beta-sheet structures.

(D) Structural superposition of the malectin-like domains of AtFER (blue) and MpFER (green).

(E) Alignment of the cytoplasmic domains of MpFER, AtERU, AtFER, and *Cr*RLK. Kinase domains are in green, putative phosphorylation sites in light blue (Ser) and violet (Thr), and the conserved catalytic Lys in red.

See also Figure S1

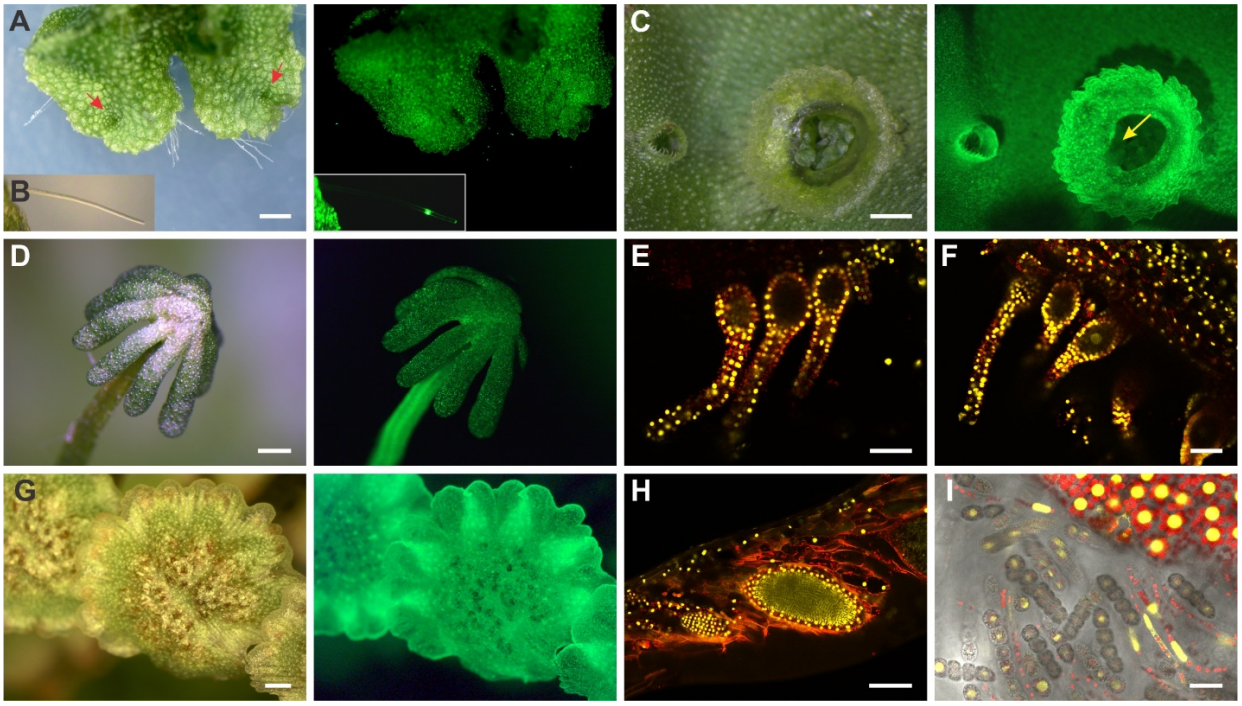

Figure 2. Mp*FER* Is Broadly Expressed in most Tissues throughout the *M. polymorpha* Life Cycle

Expression of $_{pro}$Mp*FER*:*trpVNS* in different organs of male and female *M. polymorpha* plants. Fluorescence is visualized as either green (epifluorescence microscope) or yellow (confocal microscope) color, depending on the panel.

(A to D) Bright field (left) and epifluorescence (right) images of a thallus, (A) rhizoid (C), gemmae cups (C), and an archegoniophore (D). Red arrows indicate meristematic zones, the yellow arrow gemmae. Scale bars, 0.5 mm.

(E and F) Confocal images of archegonia before (E) and 2 days after fertilization (F). Scale bar, 50 µm.

(G) Bright field (left) and epifluorescence (right) images of an antheridiophore. Scale bar, 1 mm.

(H) Confocal image of antheridia. Scale bar, 100 µm.

(I) Confocal image of sporophyte and spores. Scale bar, 25µm.

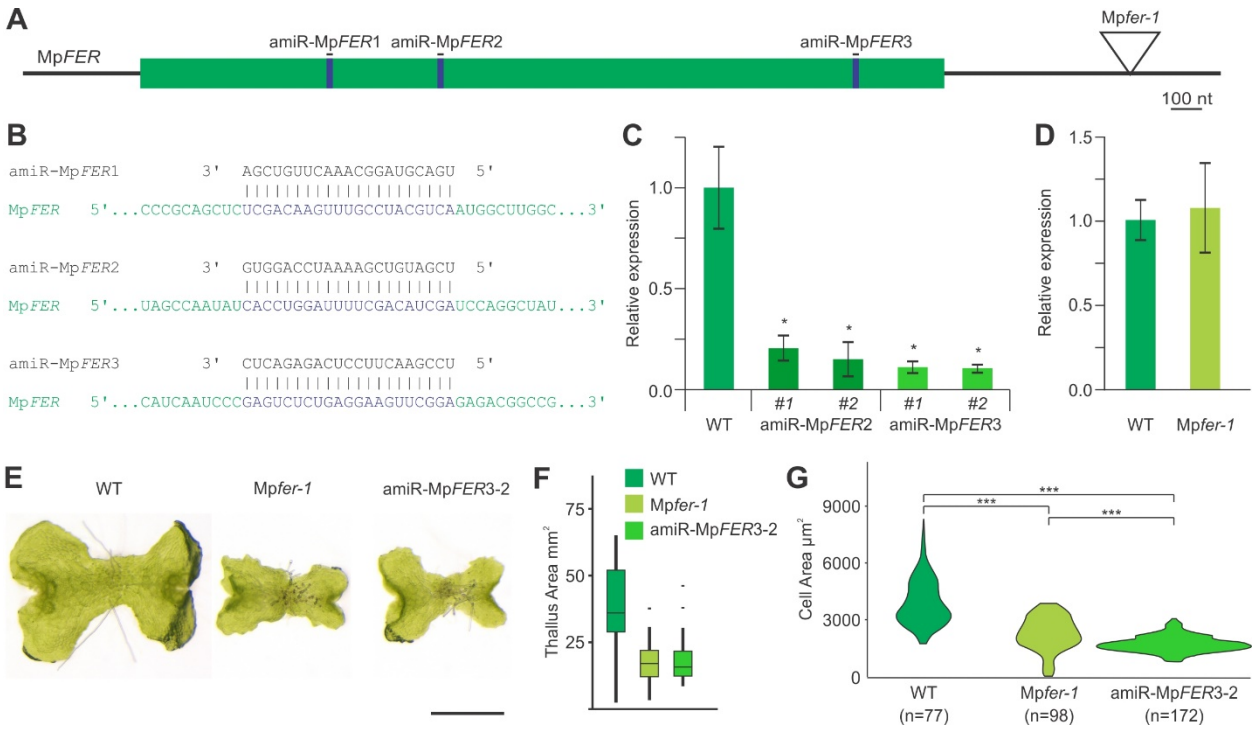

Figure 3. Mp*FER* Controls Cell Size during Gametophyte Development

(A) Representation of the mature Mp*FER* mRNA. Coding sequence are in green, locations of the amiRNA target sites in blue.

(B) Base complementary between mature amiR-Mp*FER*1, amiR-Mp*FER*2, and amiR-Mp*FER*3 with the Mp*FER* transcript.

(C) Relative expression level of Mp*FER* in thallus tissue from wild-type (WT; Tak1) and two independent insertion lines of amiR-Mp*FER*2 and amiR-Mp*FER*3, as measured by qRT-PCR. Mp*EF1* was used as internal control. Shown are means ± standard errors of the means (SEM) of three biological replicates. *P < 0.01, one-way analysis of variance (ANOVA).

(D) Relative expression level of Mp*FER* in WT and Mp*fer-1* thallus tissue, as measured by qRT-PCR. Mp*EF1* was used as internal control. Shown are means ± SEM of three biological replicates. *P < 0.01, one-way ANOVA.

(E) Representative pictures of 10-day old gemmalings of WT, Mp*fer-1*, and amiR-Mp*FER*3-2 lines. Scale bar, 1 mm.

(F) Thallus area of WT, Mp*fer-1*, and amiR-Mp*FER*3-2 lines. n = 30, outliers are indicated as black dots.

(G) Violin plot of cell size in WT, *Mpfer-1*, and amiR-Mp*FER*3-2 lines. Significant differences are indicated according to the non-parametric Kruskal-Wallis test and linear regression models (***p<0.001).

See also Figures S2 and S3

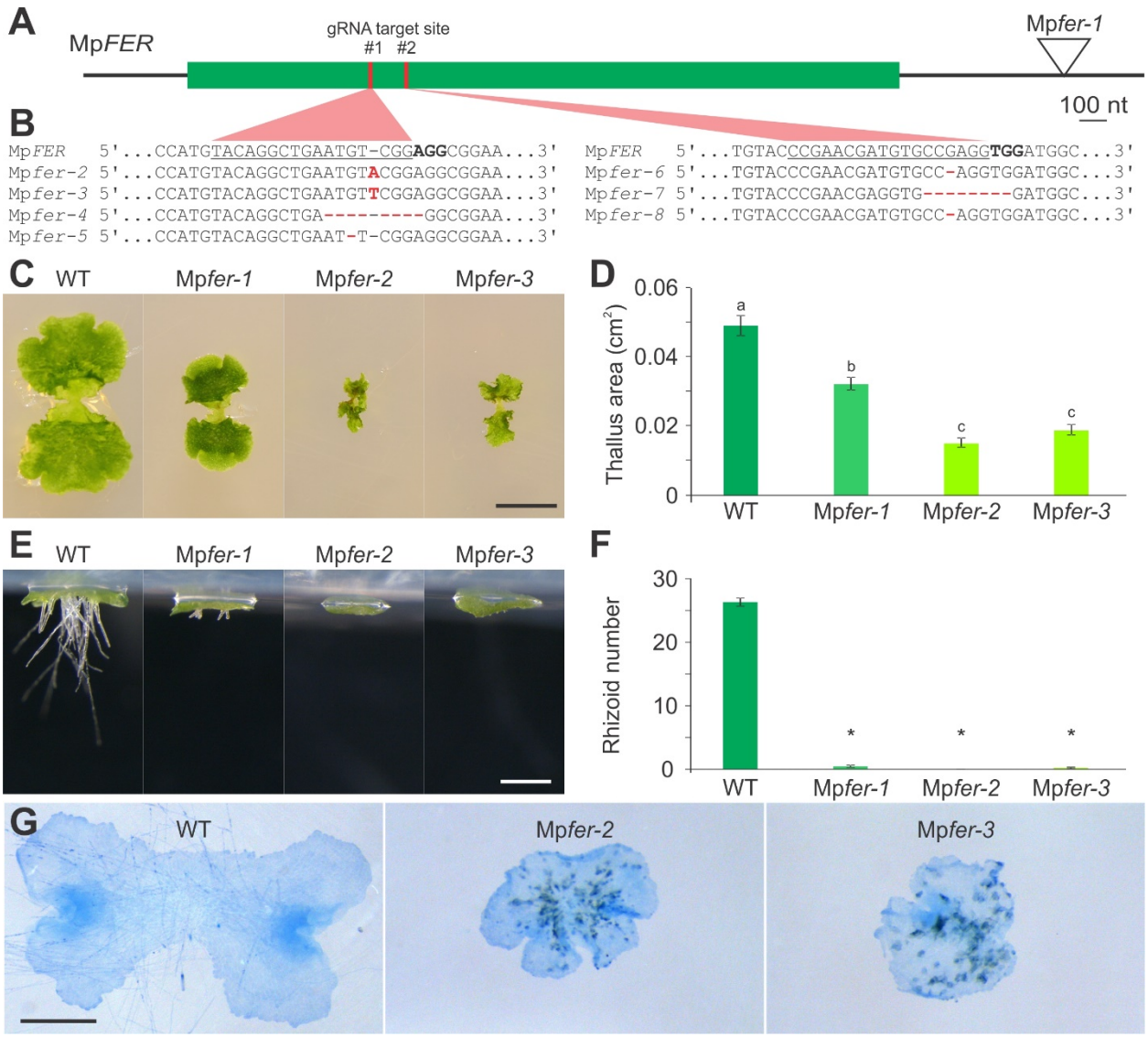

Figure 4. The Integrity of Thalli from Mp*fer* Knock-out Lines Is Severely Affected

(A) Representation of the mature Mp*FER* mRNA with the coding sequence in green, and the location of the gRNA target sites in red.

(B) Sequences of gRNA target sites in the confirmed Mp*fer* knock-out mutants. Deletions and insertions are highlighted in red.

(C) Representative pictures of 10-day old gemmalings of WT, Mp*fer-1*, and two independent Mp*fer* knock-out mutants. Scale bar, 0.5 cm.

(D) Thallus area of 10-day old gemmalings of WT, Mp*fer-1*, and two independent Mp*fer* knock-out mutants. n = 30.

(E) Representative pictures of 3-day old gemmalings growing in upside-down plates of WT, Mp*fer-1*, and two independent Mp*fer* knock-out mutants. Scale bar, 500 µm.

(F) Rhizoid number in 3-day old gemmalings of WT, Mp*fer-1*, and two independent Mp*fer* knock-out mutants. n = 30.

(G) Trypan blue staining of 7-days old gemmalings of WT, Mp*fer-1*, and two independent Mp*fer* knock-out mutants. Scale bar, 1 mm.

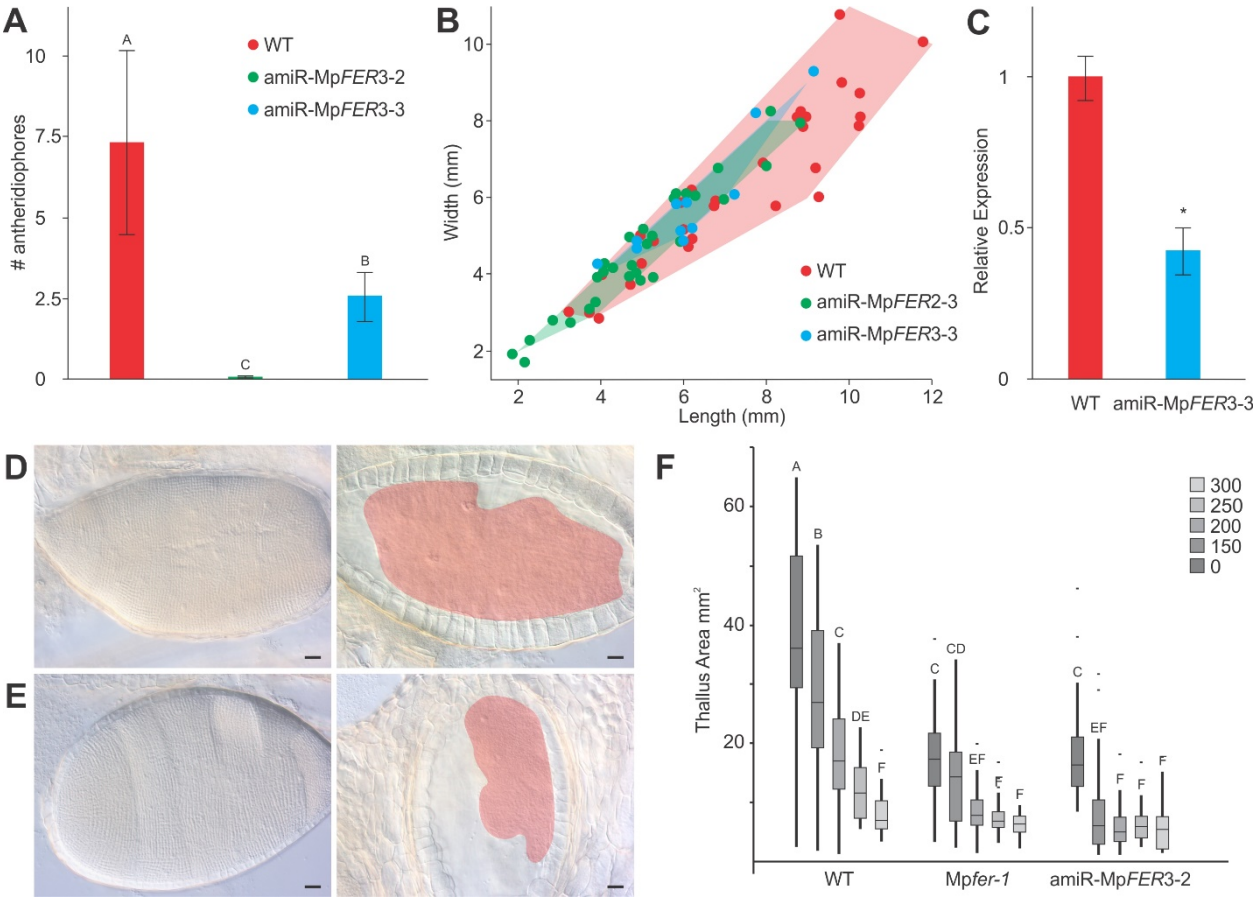

Figure 5. Conservation of *Cr*RLK1L Function in Land Plants

(A) Number of antheridiophores produced per plant for wild-type (WT, n=9) and two independent amiR-Mp*FER*3 lines (amiR-Mp*FER*3-2, n = 9; amiR-Mp*FER*3-3, n = 12). Shown are means ± SEM of two biological replicates. Means with same letter do not differ significant different with P > 0.05, one-way ANOVA, Duncan test.

(B) Antheridiophore splash platform size distribution of WT (n = 32), amiR-Mp*FER*2-3 (n = 34), and amiR-Mp*FER*3-3 (n = 11) lines. For all antheridia with a stalk >8 mm, length and width of the platform were recorded.

(C) qRT-PCR of Mp*FER* levels in antheridiophores in a WT and amiR-Mp*FER*3-3 line. Mp*EF1* was used as internal control. Shown are means ± SEM of three biological replicates. *P < 0.01, ANOVA.

(D and E) Mature antheridia of a WT (D) and amiR-Mp*FER*3-3 line (E). Bright field images (left) and in cross-section (right). The spermatogenous areas are indicated in red. Scale bar, 100μm.

(F) Thallus area of 15-day old gemmalings of WT, *Mpfer-1* mutant, and an amiR-Mp*FER*3-2 line growing on media containing different isoxaben concentrations (nM). n = 30, outliers are indicated as black dots. Shown are means ± SEM of two biological replicates. Means designated by the same letter do not significantly differ at $P > 0.05$, one-way ANOVA, Duncan test.

See also Figure S3

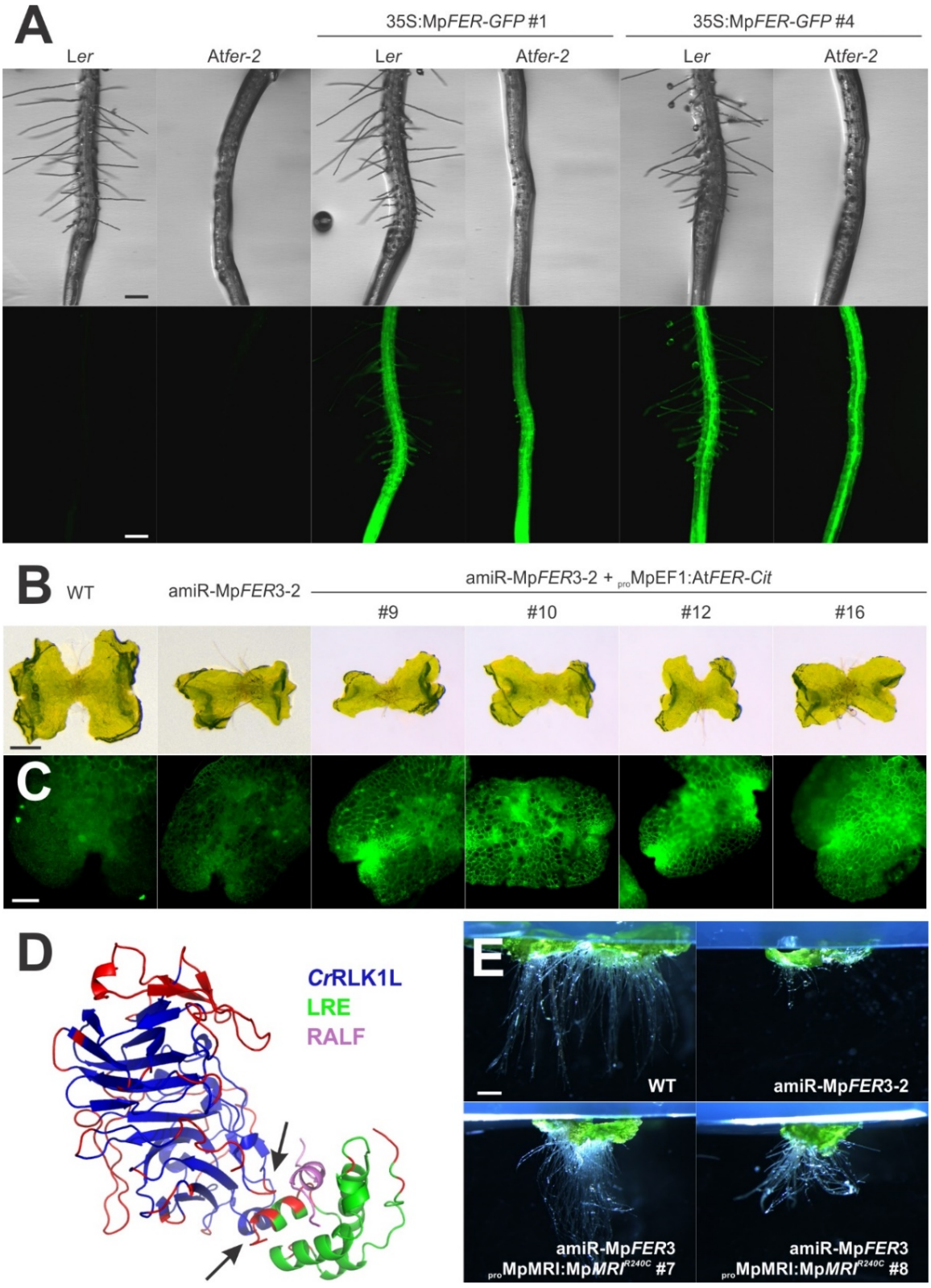

Figure 6. Interspecific Complementation of *A. thaliana* and *M. polymorpha* Plants with Reduced Levels of *FER* Activity

(A) Roots of independent *A. thaliana* lines expressing 35S:Mp*FER-GFP* in L*er* wild-type (WT) and At*fer-2* plants. Scale bar, 200 µm.

(B) 10-day old gemmalings of WT and amiR-Mp*FER*3-2 *M. polymorpha* plants with and without expression of At*FER-Cit*. Scale bar, 0.5 mm.

(C) Citrine expression in 7-day old gemmalings of WT and amiR-Mp*FER*3-2 plants with and without expression of At*FER-Cit*. Scale bar, 100 µm.

(D) Cartoon representation of the structural conservation of the *Cr*RLK1L^{ECD}/LRE/RALF complex by comparing AtFER/MpFER and AtLLG2/MpLRE1. Blue and green represent spatially highly conserved regions of *Cr*RLK1L and LRE homologs, respectively. Red indicates structural regions with low spatial conservation, lilac the C-terminal part of AtRALF23, and black arrows the interaction regions of the three proteins.

(E) Complementation of amiR-Mp*FER* lines with a dominant-active version of Mp*MRI* under its own promoter ($_{pro}$Mp*MRI*:*MRI*^{R240C}). Scale bar, 1 mm.

See also Figures S4-S7

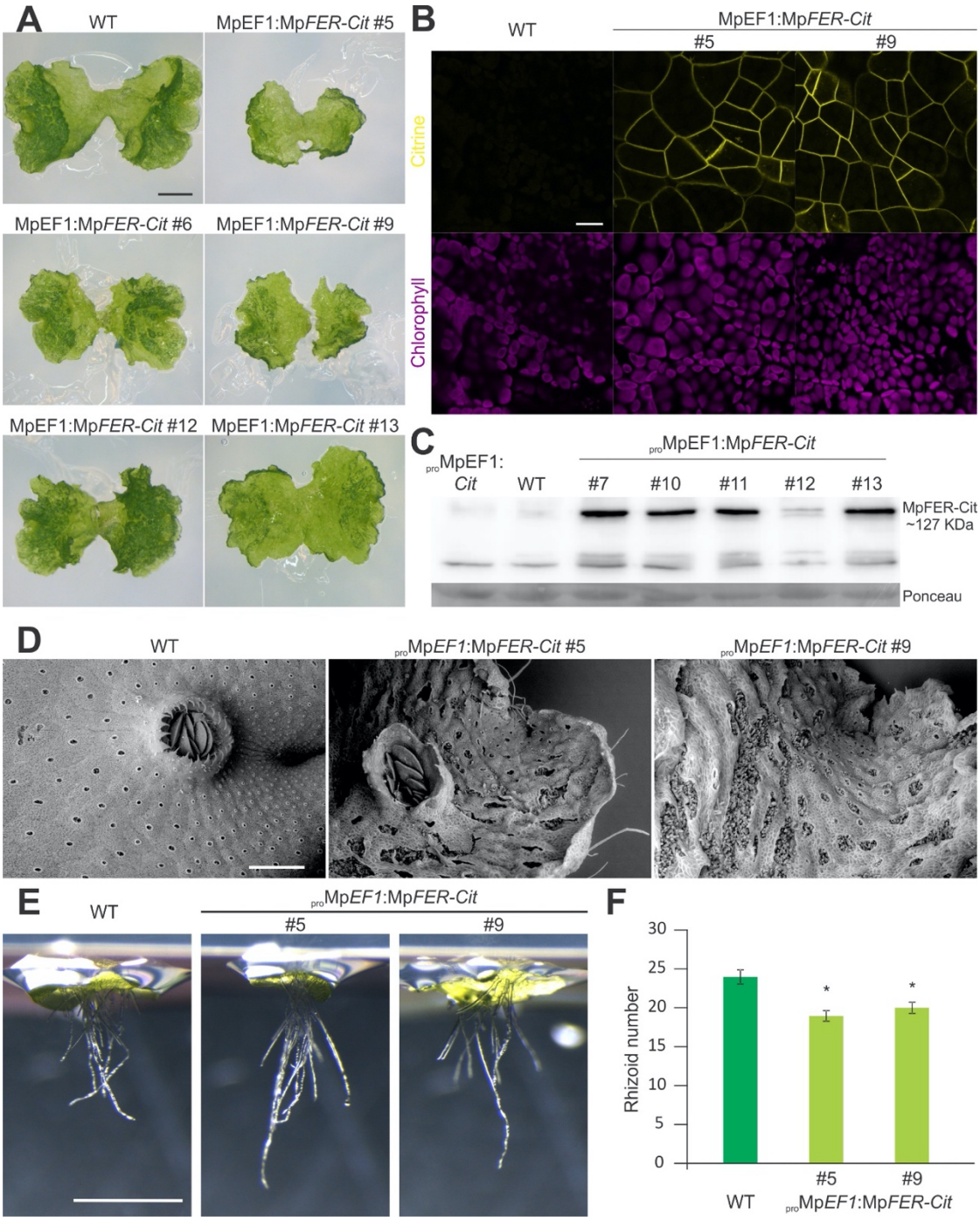

Figure 7: Overexpression of Mp*FER* Affects Morphological Integrity

(A) Representative pictures of 10-day old gemmalings of wild-type (WT, Tak1) and different lines overexpressing Mp*FER* (*pro*Mp*EF1:*Mp*FER-Cit)*. Scale bar, 1 mm.

(B) Citrine expression at the plasma membrane in WT and $_{pro}$Mp*EF1:*Mp*FER-Cit* lines *#5* and #9 as observed under confocal microscopy. Scale bar, 20 µm.

(C) Western blot analysis of $_{pro}$Mp*EF1:*Mp*FER-Cit* lines using an anti-GFP antibody. $_{pro}$Mp*EF1:Cit* and WT lines were used as positive and negative controls, respectively. The Ponceau membrane staining of the most intense band at 55 kDa (presumably Rubisco) was used as a loading control.

(D) Scanning electron microscopical images of thalli from 20-day old plants of WT and $_{pro}$Mp*EF1:*Mp*FER-Cit* lines *#5* and #9. Scale bar, 500 µm.

(E) Representative pictures of 3-day old gemmalings growing in upside-down plates of WT and $_{pro}$Mp*EF1:*Mp*FER-Cit* lines *#5* and #9. Scale bar, 1 mm.

(F) Number of rhizoids in 3-day old gemmalings of WT and $_{pro}$Mp*EF1:*Mp*FER-Cit* lines *#5* and #9. n = 30.

See also Figure S6

A

	MpFER		
% Identity	Malectin	ECD	Full protein
AtFER	33.5	31.0	43.3
AtANX1	29.8	26.5	39.8
AtANX2	30.6	27.2	40.3
AtTHE1	29.2	28.4	46.0

B

% Identity	ECD CpRLK1	CpRLK1
MpFER	25,7	29,2
Mp1g17720	35,3	45,7
AtFER	28,0	41,5

D

Qmean	$AtFER^{ECD}$
MpFER	-3.79
CpRLK1	-5.05

E

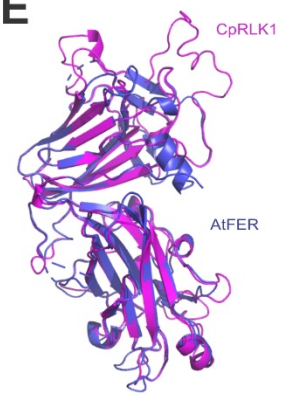

C

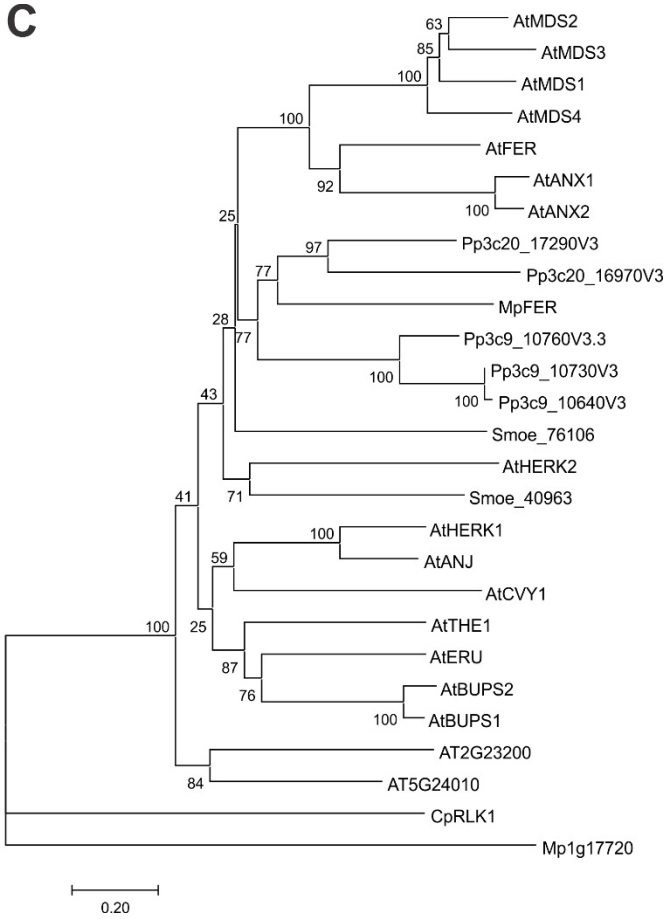

Figure S1. The *Cr*RLK1L Family Appeared together with Land Plants. Related to Figure 1.

(A) Percentage of identity of the malectin-like domain, the complete ECD, and the full protein of MpFER with AtFER, AtANX1, AtANX2, and AtTHE1.

(B) Percentage of identity of the ECD and full protein of CpRLK1 with MpFER, AtFER, and Mapoly001s0111.

(C) A rooted neighbor-joining tree of the amino acid sequence of the predicted malectin-like domain was generated using ClustalW. *Cr*RLK1L members from *Marchantia polymorpha* (Mp), *Physcomitrella patens* (Pp), *Selaginella moellendorffii* (Smoe), and *Arabidopsis thaliana* (At) were used. Algal CpRLK1 and Mapoly001s0111 were also included. The numbers indicate the bootstrap values (%) from 1000 replications. The given scale represents a substitution frequency of 0.1 amino acids per site.

(D) Qmean value for prediction of MpFER or CpRLK1 3D structures of the ECD based on the AtFER ECD. Green numbers indicate a good modelling fit, red numbers indicates a bad modelling fit.

(E) Structural superposition of the ECD of AtFER (blue) and CpRLK1 (purple).

A

Mp*miR160* Mp1g26670

GCACCTCCTCTCTCCGACTGCAGCCCGTTTCGAGATCCGAGGACTTGCTCGACGCGACTAATTGGGGAGGCCAGACTG
CACTTGCCTGGCTCCCTGTATGCCAACTGAGGAGCTCCTCAGAGACCTTGACAGGCTCCGTAGCTGGCATTCAGGGGG
CCATGCAGGAGGAAGTCGCTACCTCCCGCAAGGTGCGACTAGCTTTCTGTCTTGGGTGCACACCTCACTGATGTTTGA
TAGATTTACTTA

amiR-Mp*FER*1

TGCAAGCTTGCACCTCCTCTCTCCGACTGCAGCCCGTTTCGAGATCCGAGGACTTGCTCGACGCGACTAATTGGGGAG
GCCAGACTGCACTTGACGTAGGCAAACTTGTCGAACTGAGGAGCTCCTCAGAGACCTTGACAGGCTCCGTAGCTCGAC
ATGTTTGTCTACCTCAGGAGGAAGTCGCTACCTCCCGCAAGGTGCGACTAGCTTTCTGTCTTGGGTGCACACCTCACT
GATGTTTGATAGATTTACTTA**GGATCCATA**

amiR-Mp*FER*2

TGCAAGCTTGCACCTCCTCTCTCCGACTGCAGCCCGTTTCGAGATCCGAGGACTTGCTCGACGCGACTAATTGGGGAG
GCCAGACTGCACTTCGATGTCGAAAATCCAGGTGACTGAGGAGCTCCTCAGAGACCTTGACAGGCTCCGTAGCCACCT
GCATTTTTGACAACGAGGAGGAAGTCGCTACCTCCCGCAAGGTGCGACTAGCTTTCTGTCTTGGGTGCACACCTCACT
GATGTTTGATAGATTTACTTA**GGATCCATA**

amiR-Mp*FER*3

TGCAAGCTTGCACCTCCTCTCTCCGACTGCAGCCCGTTTCGAGATCCGAGGACTTGCTCGACGCGACTAATTGGGGAG
GCCAGACTGCACTTCCGAACTTCCTCAGAGACTCACTGAGGAGCTCCTCAGAGACCTTGACAGGCTCCGTAGCGAGTC
TGTGAGGGAGTTGGGAGGAGGAAGTCGCTACCTCCCGCAAGGTGCGACTAGCTTTCTGTCTTGGGTGCACACCTCACT
GATGTTTGATAGATTTACTTA**GGATCCATA**

B

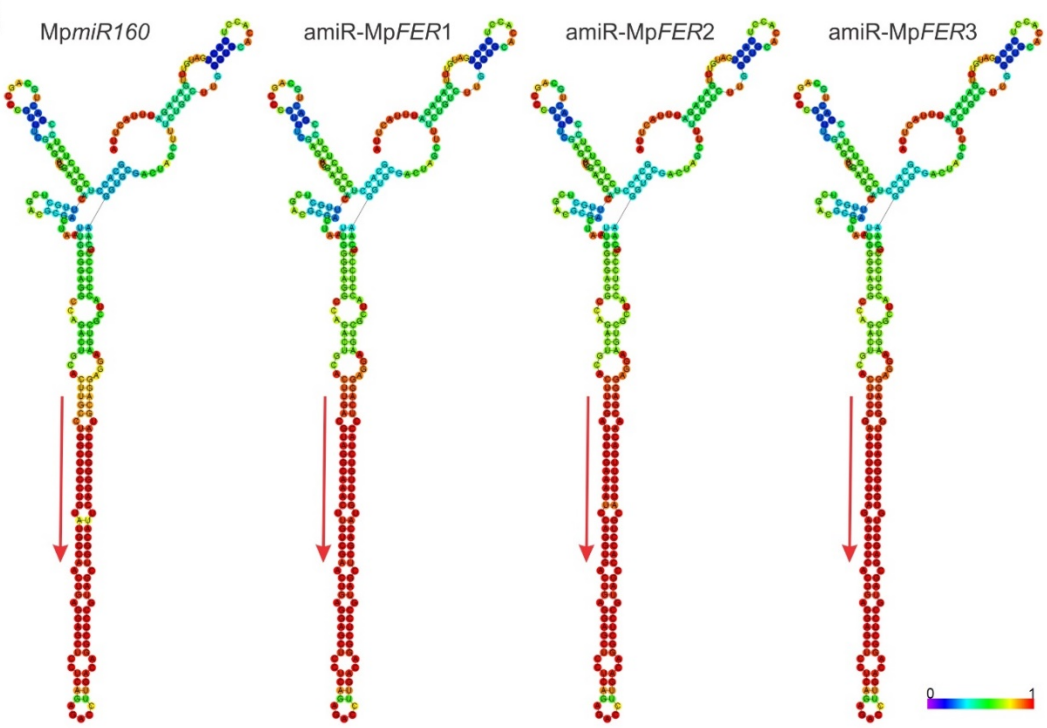

Figure S2. Design of amiR-Mp*FER* Precursors. Related to Figure 3.

(A) Mp*miR160* (Mapoly0002s0211, Mp1g26670) and amiR-Mp*FER*1, amiR-Mp*FER*2, and amiR-Mp*FER* sequences. miRNA sequences are in red and miRNA* in blue. Cloning sequences from amiR-Mp*FER* constructs are in bold.

(B) Drawing of the minimum free energy structure of Mp*miR160* and amiR-Mp*FER*3 constructs predicted by the RNAfold web server (http://rna.tbi.univie.ac.at//cgi-bin/RNAWebSuite/RNAfold.cgi). Red arrows indicate location and orientation of the mature miRNA in the precursor. The structures are colored by base-pairing probabilities; for unpaired regions the color denotes the probability of being unpaired.

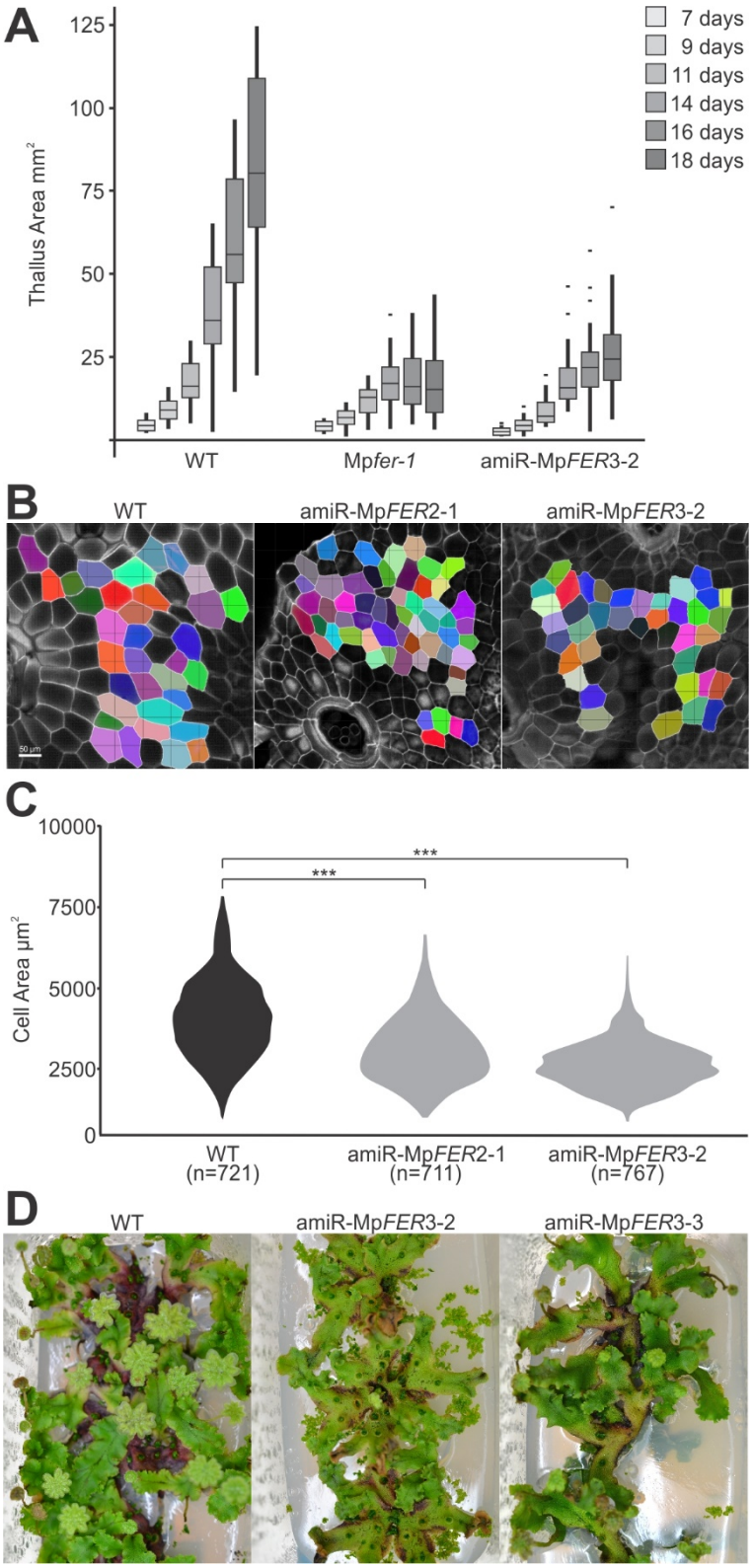

Figure S3. Reduction in Thallus and Cell Area in Plants with Reduced Mp*FER* Levels. Related to Figures 3 and 5.

(A) Thallus area of wild-type (WT), Mp*fer-1*, and amiR-Mp*FER*3-2 plants at different days after putting gemmae on plates. n = 30, outliers are indicated as black dots. Areas were estimated using ImageJ software.

(B) Representative images from cell surface areas measured in WT, amiR-Mp*FER*2-1, and amiR-Mp*FER*3-2 plants. Scale bar, 50 μm.

(C) Difference in cell size between WT, amiR-Mp*FER*2-1, *and* amiR-Mp*FER*3-2 plants is significant ($p<0.001$) based on the nonparametric Kruskal-Wallis test and a linear regression model with a highly significant interaction ($p<0.001$).

(D) Induction of antheridiophores in WT and two independent amiR-Mp*FER*3 lines. Three plants were grown in each sterile plastic box under far-red light induction.

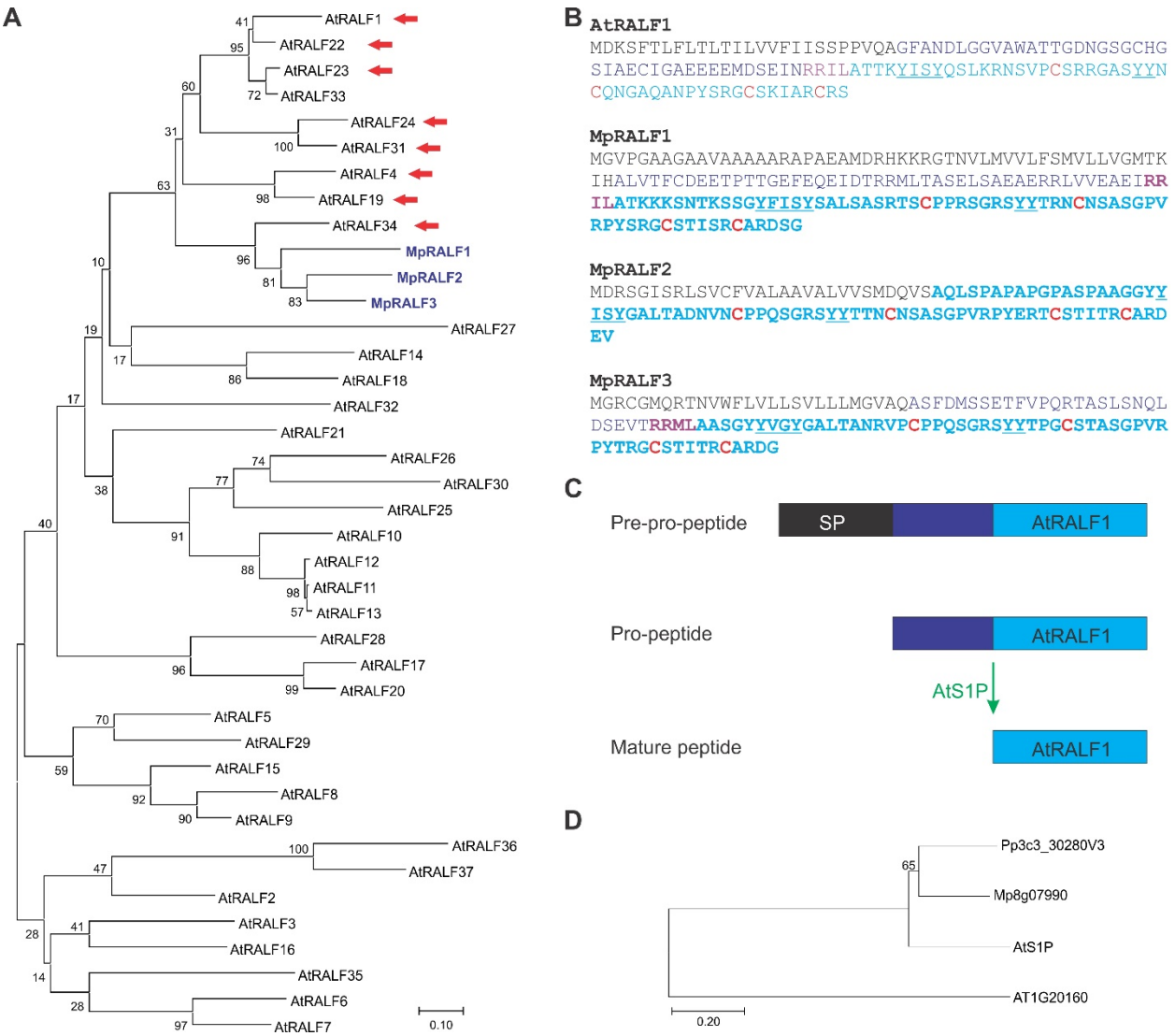

Figure S4. MpRALF Peptides Belong to the AtRALF1-clade of the RALF Family. Related to Figure 6.

(A) A rooted neighbor-joining tree of the amino acid sequence of the predicted mature RALF peptides was generated using ClustalW. RALF members from *M. polymorpha* and *A. thaliana* were used. Red arrows indicate RALFs that are known ligands of *Cr*RLK1Ls. The numbers indicate the bootstrap values (%) from 1000 replications. The given scale represents a substitution frequency of 0.1 amino acids per site.

(B) Amino acid sequence comparison of AtRALF1 and MpRALF1-3. Predicted signal peptides are in black, predicted mature peptides in light blue, conserved Cys in red, and predicted S1P recognition sites in violet.

(C) Processing pathway AtRALF1 by the S1P protease.

(D) A rooted neighbor-joining tree of the amino acid sequence of the S1P orthologs was generated using ClustalW. S1P members from *M. polymorpha*, *P. patens*, and *A. thaliana* were used. The numbers indicate the bootstrap values (%) from 1000 replications. The given scale represents a substitution frequency of 0.1 amino acids per site.

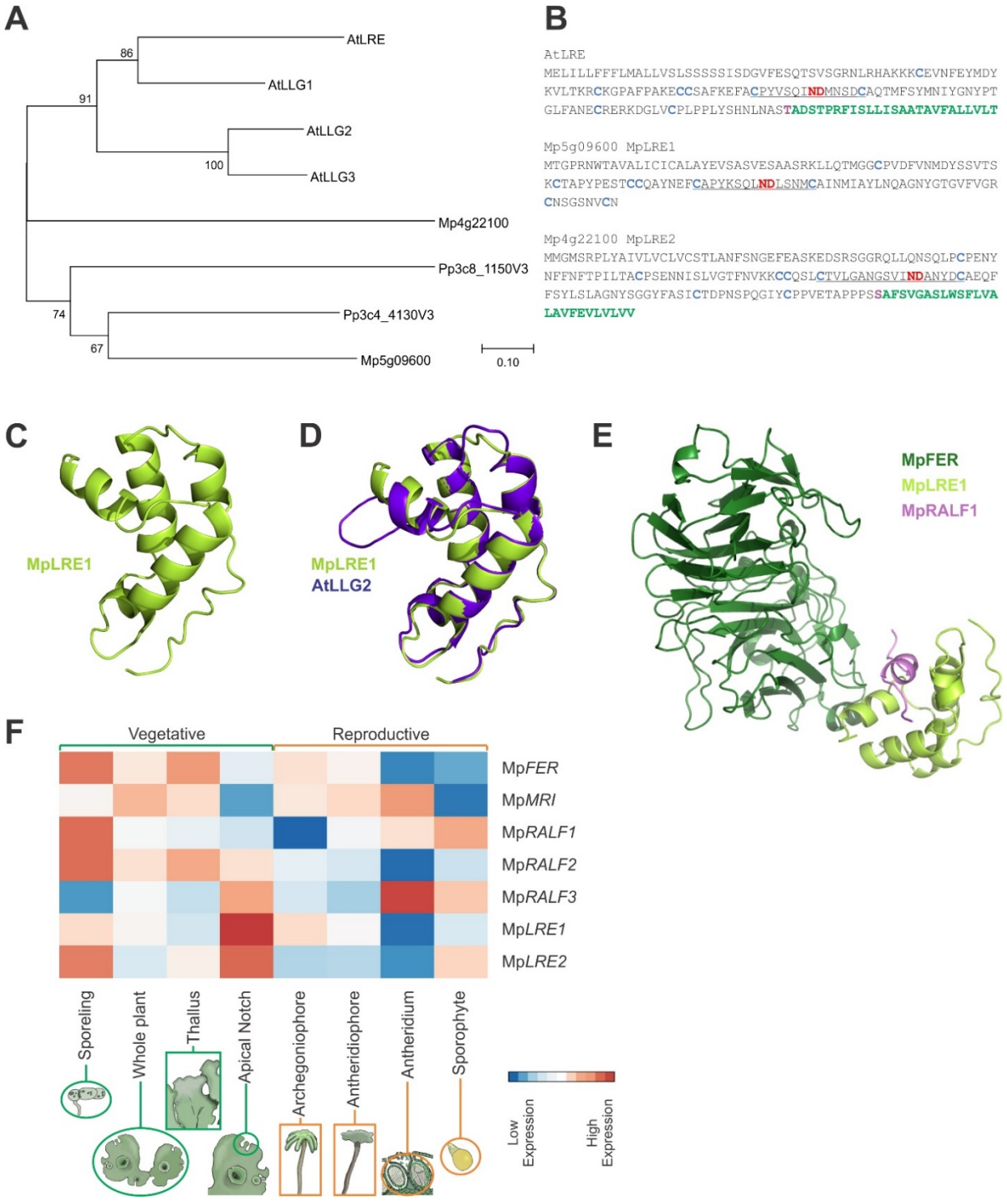

Figure S5. Two LORELEI-like Proteins Are Encoded in the *M. polymorpha* Genome. Related to Figure 6.

(A) A rooted neighbor-joining tree of the amino acid sequence of LRE orthologs was generated using ClustalW. LRE members from *M. polymorpha*, *P. patens*, and *A. thaliana* were used. The numbers indicate the bootstrap values (%) from 1000 replications. The given scale represents a substitution frequency of 0.1 amino acids per site.

(B) Amino acid sequence of AtLRE, MpLRE1, and MpLRE2. Conserved Cys are in light blue, the ND motif in red, and the GPI-anchoring site in green.

(C) Cartoon representation of the predicted 3-dimensional structure of MpLRE1, showing predicted alpha-helices.

(D) Structural superposition of AtLGG2 (blue) and MpLRE1 (green).

(E) Cartoon representation of the predicted 3-dimensional structure of the MpFER/MpLRE1/MpRALF1 complex, showing predicted alpha-helices and beta-sheets.

(F) Heatmap depicting relative gene expression based on RNAseq data (row-Z-score of vs normalized counts) of Mp*FER* and the *M. polymorpha* orthologs of At*MR*l, At*RALF1*, and At*LRE* across different tissues. Vegetative and reproductive tissues are grouped by green and orange, respectively. Averaged expression values are represented with colors of increasing red and blue intensity indicating upregulation and downregulation of gene expression, respectively.

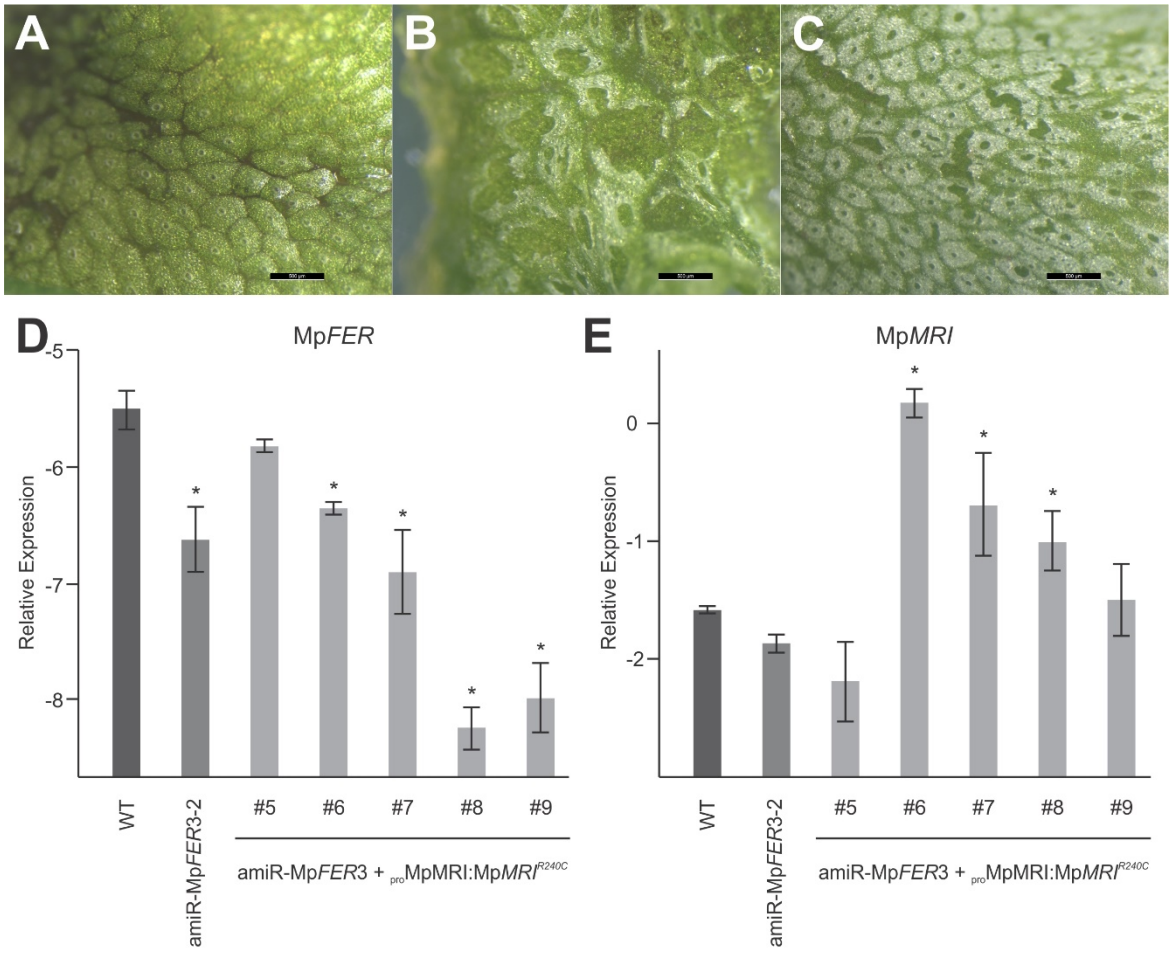

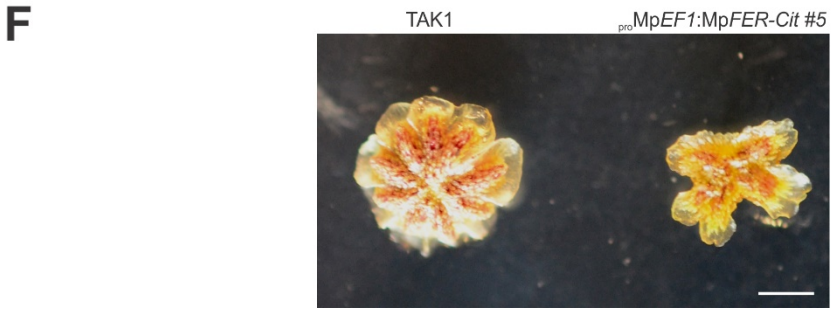

Figure S6. Expression of Mp*MRI*^{R240C} Suppresses the Bursted Rhizoid Phenotype of amiR-Mp*FER*3 Lines but Leads to Aberrant Epidermis Development. Related to Figures 6 and 7.

(A to C) Epidemical pictures of thalli from the wild-type (WT, Tak-1) (A), and amiR-Mp*FER*3 + $_{pro}$MpMRI:Mp*MRI*^{R240C} lines #6 (B) and #8 (C), which both partially suppressed the bursting rhizoid phenotype (Fig. 6).

(D and E) Relative expression of Mp*FER* (D) and Mp*MRI* (E) against the geometric mean of the reference genes Mp*ACT1*, Mp*ACT7*, and Mp*APT3* in WT, amiR-Mp*FER*3-2, and 5 lines (#5 to #9) co-transformed with the amiR-Mp*FER*3-2 and $_{pro}$MpMRI:Mp*MRI*^{R240C} constructs. Expression levels of three biological replicates were assessed by droplet digital PCR (ddPCR). The y-axis corresponds to the log2-ratio between the test and the geometric mean of the reference genes. Shown are means ± SEMs of three biological replicates. *P < 0.01, one-way ANOVA.

(F) Representative images of the antheridial receptacle of WT and $_{pro}$Mp*EF1:*Mp*FER-Cit* plants. Scale bar, 2 mm.

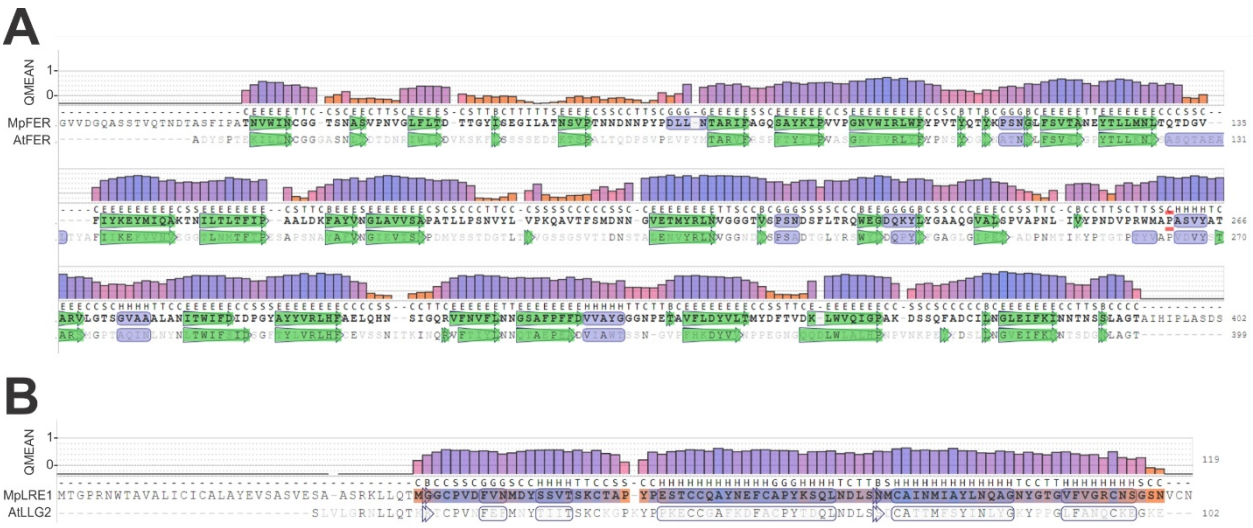

Figure S7. Structure Assessment and Quality Estimations of the MpFER and MpLRE 3-dimensional Models. Related to Figure 6.

QMEAN score barplot indicating quality estimates of the predicted models, across their aminoacidic sequence. Below the barplots, the corresponding secondary structures are displayed for both target and template sequences, with alpha-helixes represented by light purple boxes and beta-sheets by green arrows. All plots were adapted from the model report produced by the SWISS-MODEL workspace.

(A) MpFER^{ECD}, for which AtFER was used as a template (PDB 6a5b.1A).

(B) MpLRE1, for which AtLLG2 was used as a template (PDB 6a5d.1A).